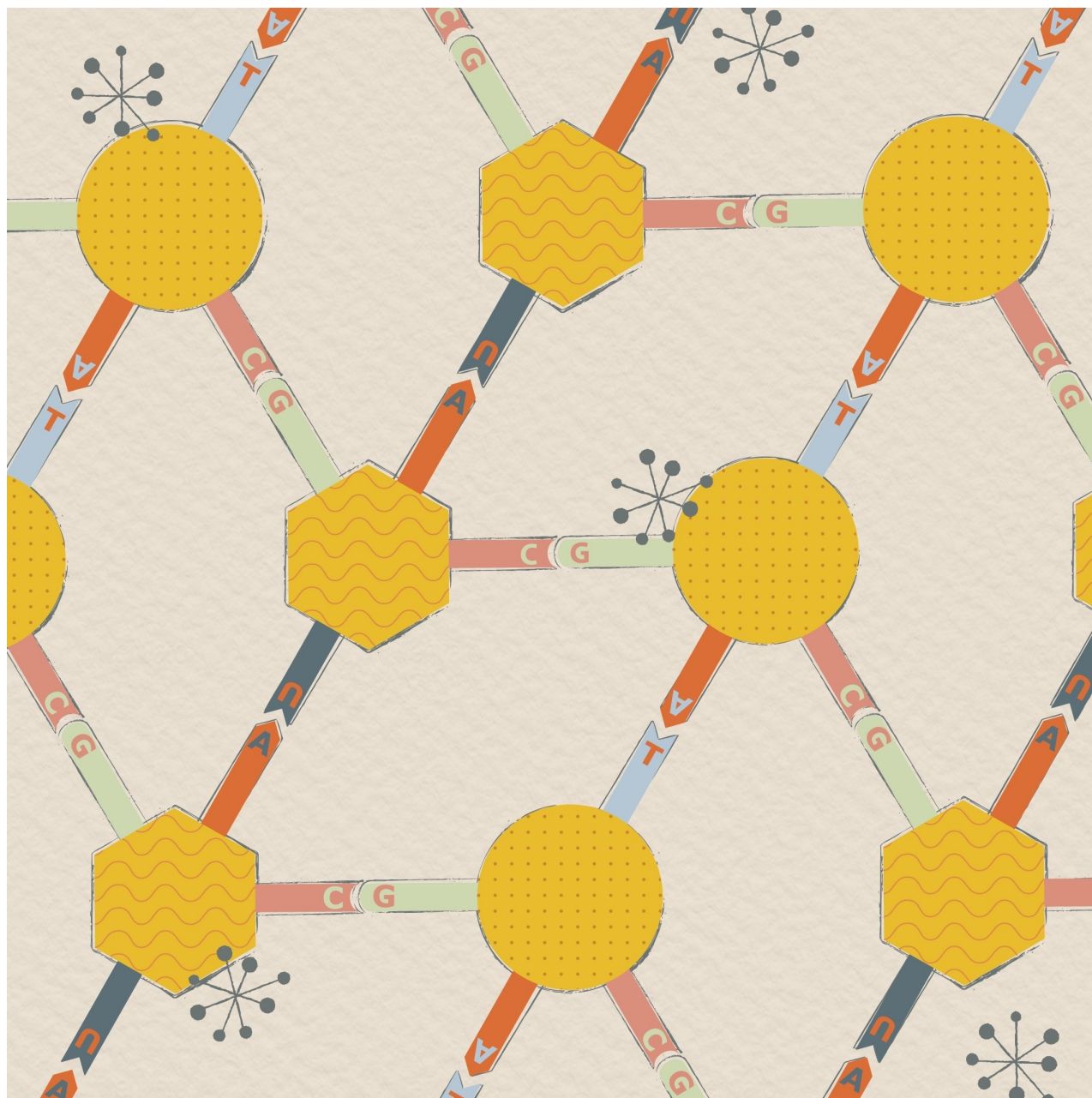


Special  
Issue

# Functional Systems Derived from Nucleobase Self-assembly

Anselmo del Prado,<sup>[a]</sup> David González-Rodríguez,<sup>\*[a, b]</sup> and Yi-Lin Wu<sup>\*[c]</sup>

Dynamic and reversible non-covalent interactions endow synthetic systems and materials with smart adaptive functions that allow them to respond to diverse stimuli, interact with external agents, or repair structural defects. Inspired by the outstanding performance and selectivity of DNA in living systems, scientists are increasingly employing Watson–Crick nucleobase pairing to control the structure and properties of self-assembled materials. Two sets of complementary purine-pyrimidine pairs (guanine:cytosine and adenine:thymine(uracil))

are available that provide selective and directional H-bonding interactions, present multiple metal-coordination sites, and exhibit rich redox chemistry. In this review, we highlight several recent examples that profit from these features and employ nucleobase interactions in functional systems and materials, covering the fields of energy/electron transfer, charge transport, adaptive nanoparticles, porous materials, macromolecule self-assembly, or polymeric materials with adhesive or self-healing ability.

## 1. Introduction

Supramolecular self-assembly organizes small components to produce patterns or structures from the bottom up. It is a simple and effective approach to create functional materials as the comprising units are brought to close proximity to interact with each other, leading to emergent and unique properties such as chromophore-chromophore electronic coupling, confined space, and cooperative binding. The intrinsic dynamic nature of non-covalent interactions further provides the system with the adaptative ability to respond to external stimuli, incoming molecules, or even structural defects. Inspired by the diverse structures and properties displayed by DNA and proteins, the development of self-assembled bioinspired and biomimetic materials has become a prosperous research field in the recent decades; achievements in biomedicine or nanotechnology are evolving to real applications. The use of bioinspired building blocks not only provides physiological compatibility/biodegradability, it also retains useful intrinsic properties (e.g. reactivity and chirality) of the small molecules in the self-assembly and allows straightforward translation of the wealth of knowledge in biomolecule interactions into fields beyond biological intent.

Among all biomolecules, nucleobases and their derivatives have provided arguably the largest number of well-controlled self-assembled architectures.<sup>[1]</sup> This is due to their unique heteroatom-rich, planar, aromatic structures, which provide strong noncovalent driving forces through metal-ligand complexation,<sup>[2]</sup>  $\pi$ - $\pi$  stacking,<sup>[3]</sup> and hydrogen (H)-bonding


interactions.<sup>[4]</sup> H-bonds are formed when a proton donor (*D*) interacts with the lone pairs of an acceptor (*A*) atom,<sup>[5]</sup> and their strength depends on the solvent (a competitor in the formation of H-bonds), the chemical nature of the *D* and *A* functions, as well as on their number and sequence in a specific molecular moiety.<sup>[6]</sup> This faithful H-bonding interaction is best seen in Watson–Crick pairing between nucleobases in DNA/RNA duplex structures. Here, hydrophobic interactions are responsible for excluding the bases from the aqueous environment and forcing them to interact by  $\pi$ - $\pi$  stacking within the same strand and by H-bonding through their Watson–Crick edges with the other strand. At this point, the matching H-bonding pattern between base pairs is the essential feature that binds two sequence-complementary strands more tightly than any other possible supramolecular structure. These complementary purine-pyrimidine Watson–Crick pairs are adenine (A)-thymine (T)/uracil (U), which bind through 2 H-bonds, and guanine (G)-cytosine (C), which associate *via* 3 H-bonds (Figure 1).


Inspired by this elegant biological design, and due to the rich chemistry and inexpensive commercial availability of nucleobases in the form of pristine bases, nucleosides (base-ribose) or nucleotides (base-ribose-phosphate), their use in supramolecular chemistry has been an early and rapidly expanding topic.<sup>[7]</sup> Two orthogonally complementary Watson–Crick pairs (A:T(U) and G:C) are available that offer

[a] Dr. A. del Prado, Prof. D. González-Rodríguez  
Departamento de Química Orgánica, Facultad de Ciencias  
Universidad Autónoma de Madrid  
28049 Madrid (Spain)  
E-mail: david.gonzalez.rodriguez@uam.es

[b] Prof. D. González-Rodríguez  
Institute for Advanced Research in Chemical Sciences (IAChem)  
Universidad Autónoma de Madrid  
28049 Madrid (Spain)

[c] Dr. Y.-L. Wu  
School of Chemistry, Cardiff University  
Park Place, Cardiff, CF10 3AT (UK)  
E-mail: WuYL@cardiff.ac.uk

 An invited contribution to a Special Collection dedicated to Functional Supramolecular Systems

 © 2020 The Authors. Published by Wiley-VCH Verlag GmbH & Co. KGaA. This is an open access article under the terms of the Creative Commons Attribution Non-Commercial License, which permits use, distribution and reproduction in any medium, provided the original work is properly cited and is not used for commercial purposes.

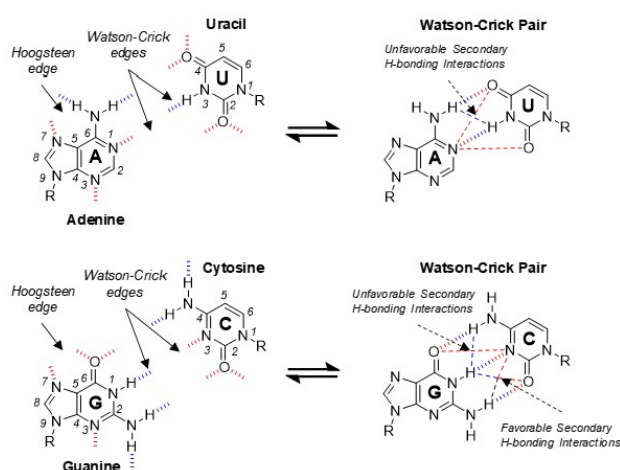


**Figure 1.** Natural Adenine (A), Uracil (U), Guanine (G) and Cytosine (C), nucleobases and their complementary Watson–Crick pairs. Dashed bonds indicate donor (*D*; blue) and acceptor (*A*; red) H-bonding sites, which may also establish favorable or unfavorable secondary interactions.

flexibility in terms of selectivity and binding strength. Taking chloroform as a reference solvent, the A:T(U) association constant is weaker by more than two orders of magnitude ( $K_a \sim 10^2 \text{ M}^{-1}$ ) than G:C pairing ( $K_a \sim 10^4 \text{ M}^{-1}$ ). This difference is due both to the presence of an additional H-bond in the G:C couple and because the H-bonding pattern in this base pair is of the ADD-DAA type, and therefore is able to establish favorable secondary interactions between adjacent H-bonding sites, as explained by the Jorgensen model (see Figure 1).<sup>[8]</sup> Due to the different H-bonding strengths in A:T(U) and G:C pairs, the latter has been often exploited to arrange molecular building blocks into structurally defined and persistent self-assemblies. On the other hand, the weaker interacting in A:T(U) advantageously allows the preparation of dynamic and adaptive systems suited for polymeric materials.

However, Watson-Crick pairing is not the only H-bonding mode established by nucleobases. Purine and pyrimidine heterocycles possess multiple protons and heteroatoms that can participate in self-assembly as H-bonding donor and acceptor units and that define diverse H-bonding edges (Figure 1). In addition, each of the nucleobases can dimerize or oligomerize. In particular, G is the base that shows higher dimerization constants ( $K_a \sim 10^3 \text{ M}^{-1}$  in  $\text{CHCl}_3$ ), larger number of H-bonding sites, and thereof the most versatile supramolecular chemistry. Lipophilic guanosines typically self-associate into a mixture of ribbon-like species by formation of different pairs of self-complementary H-bonds. However, in the presence of a size-matching cation (typically  $\text{Na}^+$  or  $\text{K}^+$ ), multiple noncovalent forces work together to yield complexes with a well-defined

number of G molecules: commonly 8, 12 or 16.<sup>[9]</sup> These G-quadruplex assemblies (Figure 2) are constituted by stacked H-bonded cyclic tetramers (G-quartets) and exhibit remarkable cooperativity and kinetic stability.<sup>[10]</sup> Besides its relevant natural role in telomere formation, G-quadruplex self-assembly is nowadays the basis of manifold applications in biological and materials sciences.<sup>[11]</sup>

As alluded to previously, nucleobases also feature versatile modes of metal coordination. For instance, T has a high affinity for  $\text{Hg}^{2+}$ , C binds  $\text{Ag}^+$  strongly, and purines A and G coordinate many soft or hard ions, such as  $\text{Au}^+$ ,  $\text{Pt}^{2+}$ ,  $\text{Pb}^{2+}$ ,  $\text{Cu}^{2+}$ ,  $\text{Zn}^{2+}$ ,  $\text{Mg}^{2+}$ , and  $\text{Ln}^{3+}$  in the absence or presence of co-ligands or nearby phosphates (in the case of nucleotides).<sup>[12]</sup> The potential metal binding site of nucleobases are shown with arrows in Figure 3. The coordination modes can be further enriched by the deprotonation form of nucleobases. Additionally, their non-coordinated positions may remain accessible to H-bonding with other species. Among all nucleobases, A is the most studied ligand<sup>[12a]</sup> due in part to the plenty nitrogen sites in its structure and in part to its more manageable solubility compared to G. When the N9 position is substituted, the N1 and N7 are primarily used for transition metal coordination via mono- and bidentate coordination modes. However, in its deprotonated form, N9 is the preferred site for coordination. Capitalized on such a feature, extended coordination structures based on A have attracted much attention.

Further to the structural aspects, it is also important to consider the energetics of the nucleobases, whose aromatic nature not only mediates  $\pi$ - $\pi$  stacking but also provide the



Anselmo del Prado received his PhD in Organic Chemistry at the Universidad Autónoma de Madrid in 2016, under the supervision of Dr. Reinecke and Dr. Elvira from the Institute of Polymer Science and Technology (Spanish Research Council). Then, he worked as postdoctoral researcher with Prof. Christoph Weder at the Adolphe Merkle Institute in Fribourg (Switzerland), where his research was focused on the preparation of supramolecular polymers and phase segregated materials for debond on-demand adhesives and self-healing materials. In 2018, he joined to the group of Prof. David González-Rodríguez at the Universidad Autónoma de Madrid. In 2019 he was awarded the Marie Skłodowska-Curie Individual Fellowship to develop self-healable materials based on cooperative supramolecular interactions.



David González-Rodríguez obtained his PhD degree in 2003 working in Subphthalocyanine Chemistry in the group of Prof. T. Torres. Between 2005 and 2008, he worked in the laboratories of Prof. E.W. Meijer at the Eindhoven University of Technology as a Marie Curie fellow. Since 2011, he leads the Nanostructured Molecular Systems and Materials (MSMn) group at the Universidad Autónoma de Madrid. He has been the recipient of numerous Grants, among them a ERC-Starting



Grant and more recently 2 ERC-Proof of Concept Grants. He has also been awarded with several prizes for young researchers: the 2010 SUSCHEM Prize, the 2011 RSEQ-Sigma Aldrich Emerging Investigator Award, the SPP-2012 Young Investigator Award, the UCM-2012 Young Researcher Award, or the 2019 Barluenga Medal. His research interests focus on the development of versatile strategies to improve or create novel functions in organic materials by rationally ordering molecules at the nanoscale using the tools of self-assembly.

Yi-Lin Wu is a Lecturer in Materials Chemistry at Cardiff University. He received his BSc from National Taiwan University in 2005 and PhD in chemistry from ETH Zürich in 2012 in the group of François Diederich. After leaving ETH, he was awarded the Swiss National Science Foundation (SNF) Fellowship to start his postdoctoral research in the group of Michael R. Wasielewski at Northwestern University, where he was subsequently appointed as the Research Assistant Professor (2014) and Research Associate Professor (2017). He takes the combined synthetic and spectroscopic approaches to interrogate the interplay between the self-assembly nanostructures and excited-state electron/energy dynamics in biology- and photovoltaics-relevant materials.



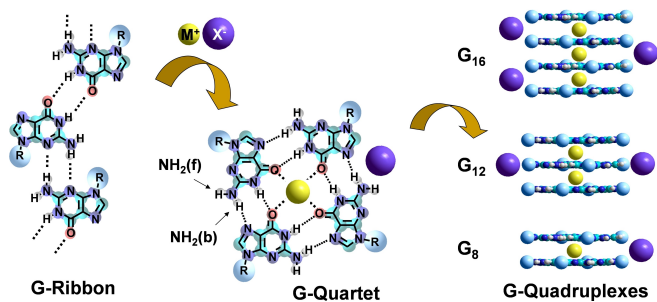


**Figure 2.** Association of guanine/guanosine molecules into ribbon oligomers or cyclic G-quartets, which can stack in the presence of cations into G-quadruplexes of diverse sizes.

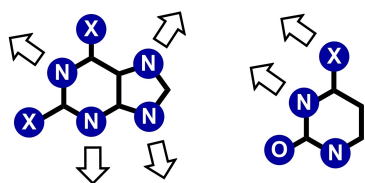


**Figure 3.** Common coordination modes/sites (highlighted with arrows) of purine and pyrimidine nucleobases.

basis for their (opto)electronic applications.<sup>[13]</sup> As in most of the organic aggregates, the energy level of self-assembled nucleobases is largely determined by the HOMO (highest occupied molecular orbital) and LUMO (lowest unoccupied molecular orbital) energies (Figure 4),<sup>[14]</sup> with perturbation by H-bonding, metal coordination and  $\pi$ -stacking interactions. The unmodified nucleobases have wide HOMO–LUMO energy gaps (3.6–3.9 eV, in the UV range). The HOMO levels follow the sequence of  $G > A > C > T > U$ , with G being most easily oxidizable (electron rich; HOMO at *ca.* –5.7 eV or 1.26 V vs. NHE). One can thus envision electron transport over the stacks of nucleobases themselves or the other aromatic substituents organized by nucleobase non-covalent interactions. The various HOMO/LUMO levels further provide selectivity for electron or hole transportation.

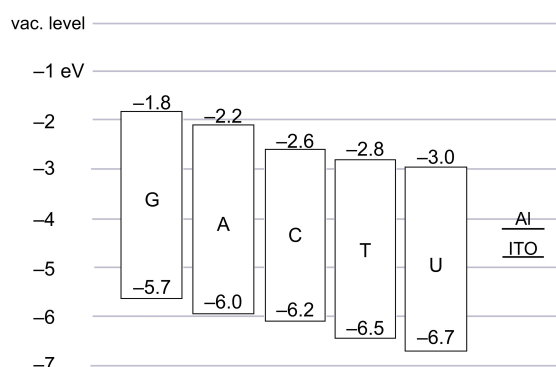


**Figure 4.** HOMO/LUMO energy levels ( $E(\text{vac})$ ) of nucleobases relative to the vacuum level, values taken from Ref. [14a]. Similar but different values in [14b,c] have been reported from different measurements. Electrochemical potential  $E(\text{SHE}) = -E(\text{vac}) - 4.44$ . Adapted from Ref. [13b] with permission. Copyright (2015) Wiley-VCH.

Therefore, two sets of complementary purine-pyrimidine pairs (G:C and A:T(U)) are available that: 1) provide selective and directional multiple H-bonding interactions, primarily, but not exclusively, through the corresponding Watson–Crick edges; 2) offer multiple coordination sites to bind to different metals; and 3) display relatively rich redox chemistry. In this review, we will highlight multiple examples that profit from these features of the nucleobases and use them in the study of energy/electron transfer phenomena, charge-transport applications, nanoparticle generation, the formation of porous materials, macromolecule self-assembly, or the generation of stimuli-responsive polymeric materials.

## 2. Energy or Charge Transporting Medium Enabled by Nucleobase Pairing

Efficient transport of excitation energy or charges across molecular components requires strong dipolar or orbital coupling. The natural tendency of nucleobases to organize themselves through H-bonding and  $\pi$ -stacking interactions provides a platform to position the energy/charge donors and acceptors in 3-D space with a high degree of control and precision. The transport events can be mediated by nucleobases or the appended substituents, resulting in functional systems to model photosynthesis or be used as chemical sensors.

### 2.1. Energy and Electron Transfer in Discrete Self-assembly

Strong association of triple H-bonds between G:C pairs has been recognized early on for organizing molecular units of different energetics to study energy and electron transfer phenomena. Such studies provided fundamental understanding of the photoinduced processes across non-bonding systems that are relevant to photosynthesis, and paved the way to the realization of molecular electronics. The pioneer work by Sessler, Ward, Barigelletti and their co-workers demonstrated excited state energy transfer from zinc-porphyrin or ruthenium-tris(bipyridyl) energy donor to free-base porphyrin or osmium-tris(bipyridyl) acceptor, respectively (Figure 5).<sup>[15]</sup> By analyzing the detailed structural and kinetic parameters, it was found that excited energy transfer can take place through the combination of Förster and Dexter mechanisms.<sup>[16]</sup> While energy transfer through the Förster channel is mediated by dipole-dipole interaction and the G:C H-bonding only serves to associate the molecular components, the observation of efficient Dexter energy transfer, which involves double electron transfers, indicates strong participation of H-bonding motifs. This observation is in line with the finding of Therien and Nocera, who showed that H-bond bridges can provide strong electronic coupling for electron transfer.<sup>[17]</sup>

Analogously, H-bonding between nucleobases has also been used to assemble electron donor–acceptor systems to model photoinduced electron-transfer processes. Electron donor/acceptor pairs of porphyrin/benzoquinone,<sup>[18]</sup> porphyrin/



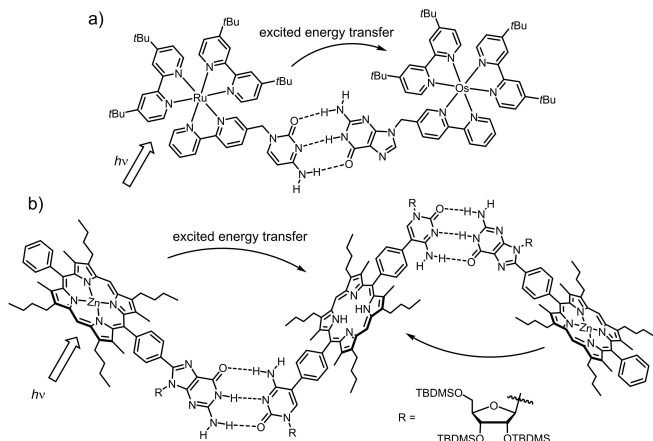


**Figure 5:** G:C-mediated excited energy transfer in a) a dimeric Ru(II) tris(bipyridyl)-Os(II) tris(bipyridyl) donor-acceptor system and b) a trimeric system composing two Zn(II) porphyrins (electron donor) and a free-base porphyrin (acceptor). TBDMS = *t*-butyldimethylsilyl.

fullerene,<sup>[19]</sup> phthalocyanine/fullerene,<sup>[20]</sup> and *N,N*-dimethylaniline/anthracene,<sup>[21]</sup> covering a wide range of charge separation ( $\Delta G_{CS}$ ) and recombination ( $\Delta G_{CR}$ ) energetics, have been linked through strong G:C H-bonds. One major thrust in the development of artificial photosynthetic model is to modulate the charge-transfer lifetime and efficiency by synthetic control.

While many of these electron donor/acceptor systems display somewhat unsatisfactorily fast charge recombination kinetics of  $k_{CR} \sim 10^9 \text{ s}^{-1}$  (ns lifetime), photoexcitation of a porphyrin-C:G-fullerene dyad ( $\Delta G_{CS} = -0.81 \text{ eV}$  and  $\Delta G_{CR} = -1.4 \text{ eV}$ , Figure 6a) generated a charge-separated radical ion pair with a very long lifetime of 2.02  $\mu\text{s}$  in  $\text{CH}_2\text{Cl}_2$ .<sup>[19]</sup> Peculiarly, the photoresponse of the dimethylaniline/anthracene pair displayed a strong dependence on the H-bond direction. When dimethylaniline-G:C-anthracene ( $\Delta G_{CS} = -0.41 \text{ eV}$  and  $\Delta G_{CR} = -2.5 \text{ eV}$ , Figure 6b) was irradiated with 400 nm laser pulses to excite the anthracene moiety, hole transfer occurs in *ca.* 30 ps,

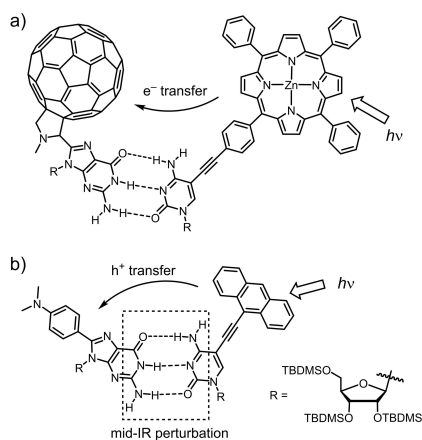


**Figure 6:** G:C-mediated photoinduced electron/hole transfer in a) a Zn(II) porphyrin–fullerene dyad and b) a *N,N*-dimethylaniline–anthracene dyad. TBDMS = *t*-butyldimethylsilyl.

as indicated by the formation of dimethylaniline radical cation by transient spectroscopy. However, in the reversed ensemble, excited dimethylaniline-C:G-anthracene does not result in the formation of a radical ion pair; exciplex emission was observed instead.<sup>[21]</sup> In addition to the directional effect, it was later found that perturbing the vibrational level of the G:C H-bonds by mid-IR pulses can decrease the yield of charge-separation.<sup>[22]</sup> All these observations have underscored the importance of *strength, planarity, and directionality* of the H-bonding motif and the subtlety in the molecular design for efficient electron transfer.

In addition to G:C base pairs, other nucleobase H-bonding interactions have also been used for electron donor–acceptor assemblies. For instance, quenched phthalocyanine fluorescence was found in the self-assembly of tetra-A Zn-phthalocyanine (donor) and T-anthraquinone (acceptor).<sup>[23]</sup> Taking this concept further, the Zhu group developed a sensing scheme based on fluorescence restoration.<sup>[24]</sup> It was found that photoinduced electron transfer occurs in the self-assembly of pyrene-A:T-TTF (TTF = tetrathiafulvalene) or pyrene-T:A-nitronyl nitroxide dyads to quench the pyrene emission.

Fluorescence intensity was recovered in the presence of, respectively, other alkylated T or A components (Figure 7a). However, since it was the same kind of A:T base-pairing interaction in the competition of binding, only moderate sensitivity was observed. In addition to canonical Watson–Crick interactions, D'Souza and Ito reported an ensemble of U-functionalized  $\text{C}_{60}$  and 2-aminopurine (2-AP), a fluorescent purine analogue of guanine and adenine (Figure 7b). In this system, 2-AP is itself a H-bonding motif and an intrinsic electron donor (+0.26 V vs.  $\text{Fc}^+/\text{Fc}$ ); thus, the self-assembly has  $\Delta G_{CS} = -2.0 \text{ eV}$  from excited 2-AP or  $\Delta G_{CS} = -0.4 \text{ eV}$  from excited  $\text{C}_{60}$ , and  $\Delta G_{CR} = -1.3 \text{ eV}$ . Excitation of the system at 355 or 532 nm in a  $\text{CH}_2\text{Cl}_2$ - $\text{CH}_3\text{OH}$  mixture resulted in the formation of 2-AP $^{\bullet+}$ :U- $\text{C}_{60}^{\bullet-}$  radical ion pairs with a charge recombination rate of  $k_{CR} = 6 \times 10^6 \text{ s}^{-1}$ .<sup>[25]</sup> This kinetic parameter is three orders of magnitude slower than

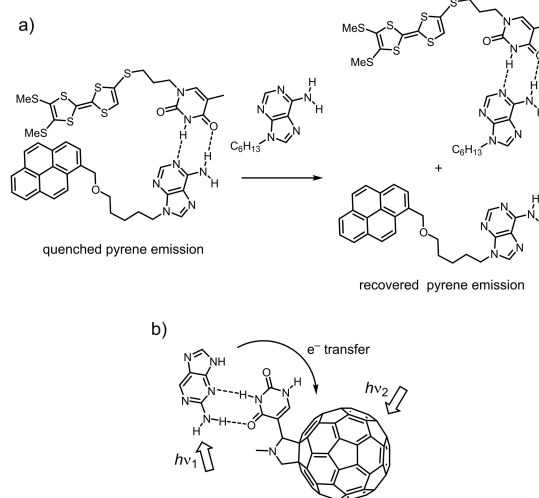


**Figure 7:** Photoinduced electron transfer mediated by a) a A:T pair in TTF-T:A-pyrene to quench pyrene emission, and b) a purine:U pair in 2-aminopurine:U-fullerene to give long-lived charge-separated ion pairs.

its  $k_{CS}$  and is similar to that of the porphyrin-C:G-fullerene dyad (Figure 6a).<sup>[19]</sup> In both cases, the slow  $k_{CR}$  may be ascribed to the large  $\Delta G_{CR}$  and small reorganization energy characteristics of the spherical  $C_{60}$  moiety.<sup>[26]</sup>

Exploiting metal-induced G-quadruplex formation, Wu and Wasielewski studied the photoinduced hole transfer processes in size-defined G-quadruplexes that are peripherally functionalized with electron acceptors.<sup>[27]</sup> In these nanostructures, self-H-bonding guanines are intrinsic electron donors (ca. +1.2 V vs. SCE)<sup>[14c,28]</sup> to be photo-oxidized by the excited electron acceptors. While the photosynthetic model systems presented earlier possess only one electron donor (e.g. porphyrin, pyrene, or 2-aminopurine) to serve as the hole trap, multiple guanine units in G-quadruplexes provide additional sites, that are either H-bonded or  $\pi$ -stacked relative to each other, for the oxidizing equivalents to migrate over.

The photoinduced charge-separation state of a G-erylene diimide (G-PDI) conjugate was found to survive more than hundred folds longer upon the formation of the G-quadruplex as compared with the monomeric G-PDI dyad (Figure 8).<sup>[27a]</sup> Due to the prominent spectroscopic feature associated with PDI anions, this significant lifetime extension was attributed largely to electron delocalization/co-stabilization by the co-facially stacked PDI moiety. In a continued study where the acceptor  $\pi$ -stacking is minimized, Wu and Wasielewski explored a G-based triad composed of an 8-(4'-aminophenylethynyl)guanine (GEAn) electron donor covalently attached to a 4-aminonaphthalene-1,8-imide (ANI) chromophore and a naphthalene diimide (NDI) electron acceptor (GEAn-ANI-NDI, Figure 8).<sup>[27b]</sup> Photoexcitation of the ANI moiety leads to two-step charge transfer  $GEAn^{-1*}ANI-NDI \rightarrow GEAn^{\bullet+}-ANI^{\bullet-}-NDI \rightarrow GEAn^{\bullet+}-ANI-NDI^{\bullet-}$ . In comparison with the monomeric triad, charge recombination in this G-quadruplex is slowed by enhanced radical-pair intersystem crossing driven by the greater electron-nuclear hyperfine interactions in the G-quadruplex assembly. Moreover, time-resolved EPR spectro-

scopy shows that the spin-spin-exchange interaction ( $J$ ) between the radicals of  $GEAn^{\bullet+}-ANI-NDI^{\bullet-}$  within the G-quadruplex is smaller than that of the monomer, suggesting that the spin (charge) density in  $GEAn^{\bullet+}$  is more dispersed over the nucleobases. The spectroscopic results are consistent with hole sharing among guanines within the G-quadruplex<sup>[29]</sup> that is kinetically competitive with the formation of  $GEAn^{\bullet+}$ . Such a result reveals the possibility of nucleobase-arene assembly for lifetime engineering by using supramolecular design.<sup>[30]</sup> This also suggests that G-quadruplexes can serve as a hole trap mitigating oxidative DNA stress and effective hole conduits in ordered donor-acceptor assemblies (see Section 2.2).

## 2.2. Charge Transport Through the Solids of Nucleobases or Nucleobase-Arene

Charge transport through the DNA base stack has been an interesting topic of study from both the biological and nanotechnology points of view.<sup>[13a,31]</sup> While charge transport occurs along the stack primarily through the intrastrand pathways in DNA, the charge carriers can also migrate to the neighboring site over the H-bond bridges, as alluded to in the previous section. Such a property of nucleobases has been exploited by Maruccio and co-workers in field-effect transistors based on deoxyguanosine derivatives.<sup>[32]</sup> Guanosine was chosen for its lowest oxidation potential among the DNA bases and strong self-association, which favors carrier transport and self-assembly, respectively. In a planar metal-insulator-metal nanojunction, guanosine derivatives self-assembled into a ribbon structure and displayed current-voltage character as in a p-channel MOSFET (Figure 9).<sup>[32b]</sup> The current rectification is believed to be to some extent caused by the overall dipole of the guanosine ribbon, whose orientation was not controlled in these devices. While the detailed H-bonding structure was not analyzed, the other nucleobases (A, T, U, C) have also been applied as the carrier transporting and blocking layers in organic light emitting diodes (OLED), primarily for their appropriate electronic energy levels.<sup>[13b,33]</sup>

Ionic complexes composed of nucleobases that display semiconductive or metallic behavior can be produced with the assistance of H-bonding interactions. The formation of hemiprotonated C dimer ( $C\cdot H-C^+$ ) and H-bonding between columns of C and substituted 7,7,8,8-tetracyanoquinodimethane (TCNQ) was suggested to provide part of the driving force for the formation of radical ions of the latter component in crystals.<sup>[34]</sup> The nature of the substituent in R-TCNQ strongly affects the degree of charge separation and hence electrical conductivity of the products. Among the wide series of complexes isolated, Murata *et al.* found that the fully ionic charge-transfer (CT) salts of  $(CHC^+)(TCNQ^{\bullet-})$  and  $(CHC^+)(Et_2TCNQ^{\bullet-})$  exhibit electrical conductivity of  $\sigma_{RT} = 10^{-4} - 10^{-2} \text{ S cm}^{-1}$ , and the partially ionic or mixed-valent CT salt of  $(CHC^+)(MeTCNQ^{0.5\bullet-})_2$  shows metallic character, with  $\sigma_{RT} = 2.7 - 7.2 \times 10^1 \text{ S cm}^{-1}$  (Figure 10a). The high conductivity for the fully ionic salts was somewhat unexpected and was ascribed to the large overlap integral in the TCNQ

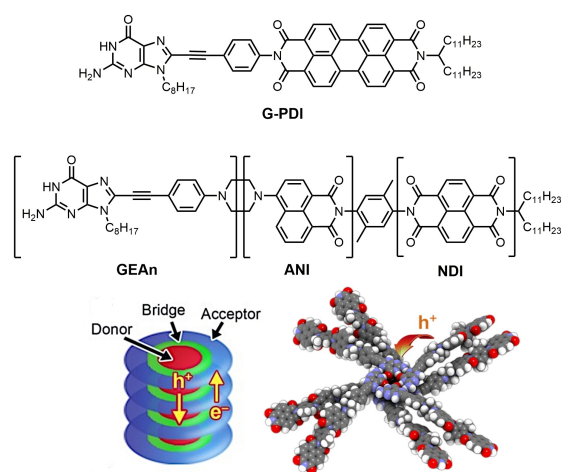


**Figure 8.** G-quadruplex self-assemblies with the concentric arrangement of electron-rich G (core) and electron-poor moieties (PDI or ANI-NDI, periphery) for independent hole and electron transport. Adapted from Ref. [27] with permission. Copyright (2013 and 2015) American Chemical Society.

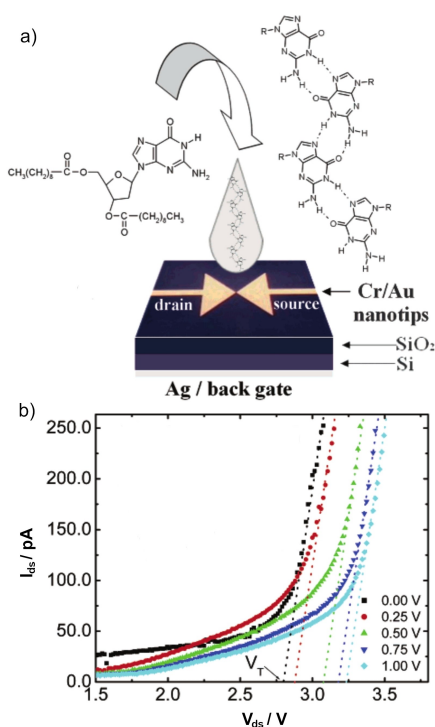


**Figure 9.** a) Self-assembly of an acylated G derivative on a three-terminal device, consisting of 2 arrow-shaped Cr/Au electrodes on a SiO<sub>2</sub> substrate and a third Ag back electrode. b) Characteristic drain–source current ( $I_{ds}$ ) dependence on the voltage ( $V_{ds}$ ) at discrete gate voltages ( $V_g$ , values shown in the legends). Adapted from Ref. [32b] with permission. Copyright (2003) American Chemical Society.

column caused by a short interplanar distance ( $d=3.14$  Å, Figure 10b and c).

Covalently linking strongly electron rich TTF to an uracil moiety (TTF-U) provides specific structural control of the conducting column in the solid-state assemblies.<sup>[35]</sup> The black-green microcrystalline solids composed of TTF-U and 7,7,8,8-tetracyanoquinodimethane (TCNQ) show characteristic low-energy CT absorption around 3000 cm<sup>-1</sup> and room-temperature

conductivity  $\sigma_{RT}=0.07$  S cm<sup>-1</sup> (Figure 10). Vibration analysis of the nitrile band suggests the partial (0.7) electron transfer accompanied with CN...H–N between TTF-U and TCNQ units. In an analogous study, self-supporting films of bis(TTF)-guanosine (TTF<sub>2</sub>-G) derivatives were oxidized by TCNQ; the film exhibits an X-ray diffraction pattern consistent with segregated TTF/TCNQ 1D-chain alignment and moderate electrical conductivity ( $\sigma_{RT}=0.0366$  S cm<sup>-1</sup>).<sup>[36]</sup>

Self-assembled, conductive materials can also be prepared by attaching large  $\pi$ -conjugated moieties (“organic semiconductor”) to nucleobases. Barbarella and co-workers reported dinucleotide-oligothiophene conjugates, where the latter is often employed as the active component in organic electronics.<sup>[37]</sup> The self-ordering dinucleotide moieties are either attached at both terminal positions of quaterthiophene (AA, TT, or AT) or on the central unit of quinquethiophene (CG or TA, Figure 11). The amphiphilic nature of these molecules allows the control of their solid-state morphology. Due to the complicated conformation about the dinucleotide units, the exact H-bonding mode between nucleobases is unclear; nevertheless, luminescent rod or quadrangular-plate crystals can be obtained with a high degree of homogeneity. By injecting electrons from Au finger electrodes, space-charge limited current (SCLC) measurements revealed hole mobilities ranging from  $2.4 \times 10^{-8}$  to  $5.8 \times 10^{-6}$  cm<sup>2</sup> V<sup>-1</sup> s<sup>-1</sup>. Such values are a few orders of magnitude lower than the analogous oligothiophenes. However, the wide range of hole mobility reflects that distance and regularity between oligothiophenes are subtly determined by the dinucleotide self-assembly.<sup>[37b]</sup>

It is conceivable that the large number of flexible carbon–carbon single bonds in Barbarella’s dinucleotide-oligothiophene conjugates hampers thiophene–thiophene interactions, as nucleotides in some conformers would locate atop the thiophene face and hence prevent continuous thiophene stacking. The necessity of long-range chromophore stacking was nicely demonstrated in a [NDI-A]<sub>10</sub>:dT<sub>10</sub> system by the Govindaraju group.<sup>[38]</sup> NDI units  $\pi$ -stack in this co-assembly driven by complementary Watson–Crick base pairing and

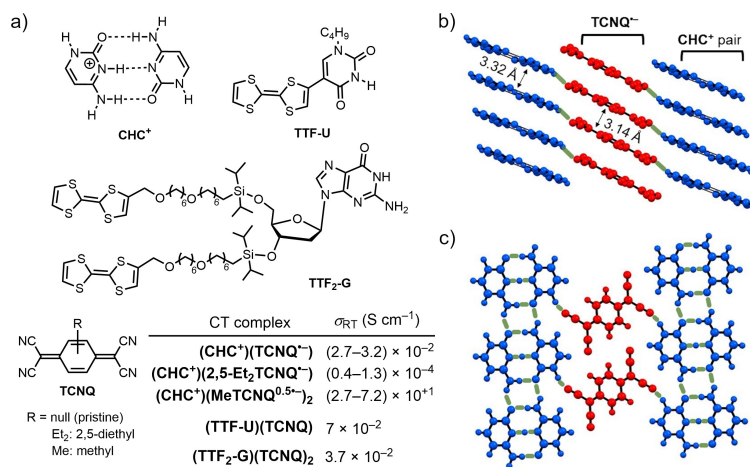


**Figure 10.** a) Conductive intermolecular charge-transfer complexes between nucleobase and TTF and/or TCNQ derivatives. b) Segregated columnar arrangement of TCNQ<sup>-</sup> (red) and CHC<sup>+</sup> pair (blue) of (CHC<sup>+</sup>)(TCNQ<sup>-</sup>). c) H-bond sheet of (CHC<sup>+</sup>)(TCNQ<sup>-</sup>). Green lines indicate H-bond.



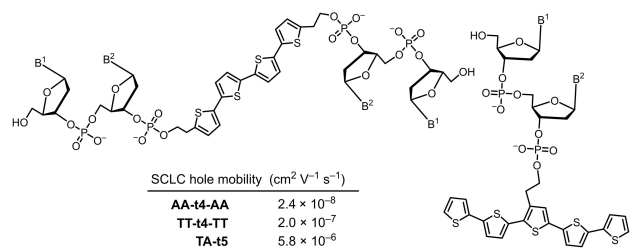


**Figure 11.** Dinucleotide-oligothiophene conjugates displaying hole conductivities by space-charge limited current (SCLC) measurements. B<sup>1</sup> and B<sup>2</sup> = nucleobases; t4 = quaterthiophene (left) and t5 = quinquethiophene (right).

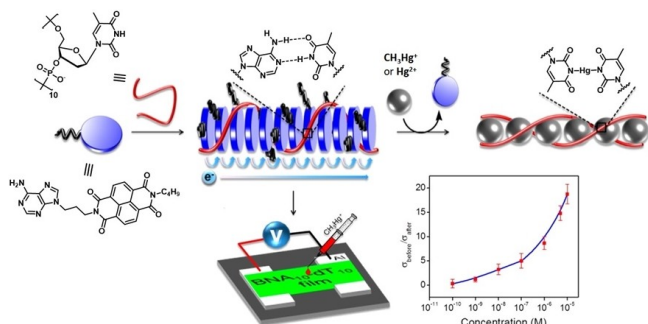


**Figure 12.** Ordered  $\pi$ -stacking of the NDI units of NDI-A, assisted by the formation of [NDI-A]<sub>10</sub>:dT<sub>10</sub> assembly, resulting in n-type conductivity. Conductometric detection of Hg<sup>2+</sup> can be made possible due to the disruption of A:T H-bonding by T-Hg-T coordination. Adapted from Ref. [38] with permission. Copyright (2016) American Chemical Society.

hydrophobic interactions, and give n-type transport property with mobility on the order of  $\mu_{\text{FET}} \sim 10^{-3} \text{ cm}^2 \text{V}^{-1} \text{s}^{-1}$  measured in FET devices or conductivity of  $\sigma \sim 10^{-6} \text{ S cm}^{-1}$  measured

between two Al electrodes. Lowering of electric conductivity of this self-assembly system can be used to detect mercury ( $\text{CH}_3\text{Hg}^+$  or  $\text{Hg}^{2+}$ ) due likely to the [dT-Hg-dT]<sub>n</sub> duplex formation, which results in much less ordered NDI-A aggregates (Figure 12).

### 3. Porous Materials Based on Nucleobase H-Bonding or Metal Coordination

#### 3.1. Adaptive Self-assembled Nanoparticles

Nucleobases are prone to coordinate with metal ions through the heteroatoms in the ring structure. Since the discovery of such phenomena, a large number of researches have been devoted to understanding and controlling such interactions. For an overview of the structural aspect, we refer readers to recent reviews for more detail.<sup>[12a,b,d,39]</sup> Among all nucleobase coordinating metal ions, lanthanides are unique as they exhibit large coordination numbers and high coordination flexibility. Such a characteristic permits the self-assembly of lanthanides and adenosine/guanosine monophosphate in particular, leading to amorphous nanoparticles (Figure 13a).<sup>[40]</sup> Binding to phosphate is critical to this process as none of the nucleobases alone would form nanoparticles with lanthanides. The abundant and flexible modes of interaction is the key of nanoparticle formation. As a matter of fact, it has been reported that, aggregation of self-H-bonding guanosine monophosphate can be the precursor to highly fluorescent carbon dots.<sup>[41]</sup>

The resultant nanoparticles feature adaptive coordination networks that are capable of capturing guest molecules of various charge, size and shape.<sup>[42]</sup> Luminescence turn-on can be

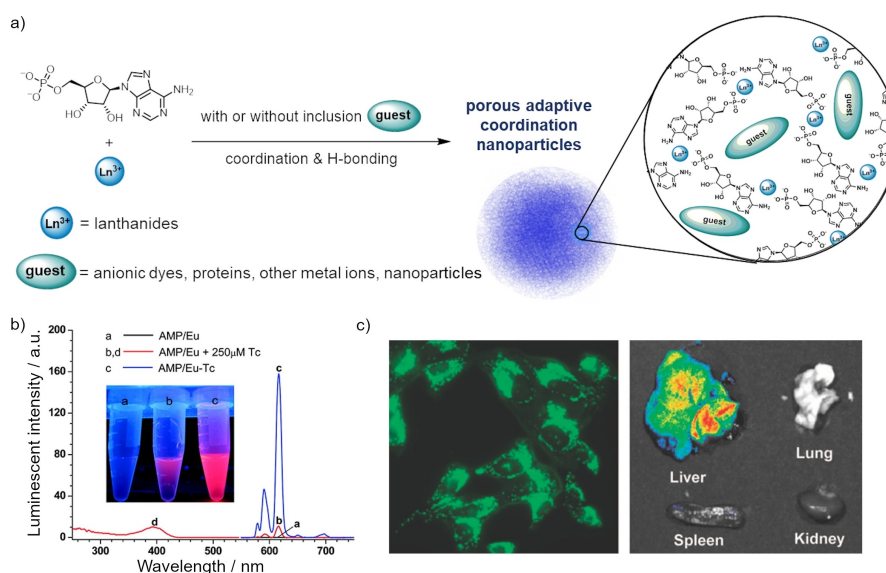


**Figure 13.** a) Formation of porous coordination nanoparticles from nucleotides and lanthanide ions. AMP is shown as an example. The flexible coordination to  $\text{Ln}^{3+}$  allows adaptive pore structures that can capture guest molecules of various charge, size and shape. b)  $\text{Eu}^{3+}$  emission from the AMP/Eu nanoparticles in the presence or absence of tetracycline (Tc). c) Fluorescence images of perylene-3,4,9,10-tetracarboxylate doped AMP/Gd nanoparticles added to HeLa cells (left) or tissues of injected mice (right). Adapted from Ref. [42b and 45] with permission. Copyright (2009 and 2012) American Chemical Society.

achieved using these nucleobase nanoparticles. For instance, when a cyanine dye was incorporated in AMP/Gd<sup>3+</sup>, intense blue emission  $\Phi_F \sim 49\%$  was observed by the Kimizuka group, whereas the same dye in water displays very weak emission (< 1%).<sup>[42a]</sup> Such enhancement was attributed to the restricted energy-dissipating internal motion of the dye in the confined environment of the nucleobase nanoparticles. Alternative approaches take the advantage of energy transfer processes from either the excited nucleobase or the incorporated dye to the lanthanide. The former scenario was demonstrated in the capability of AMP/Tb<sup>3+</sup> to detect Ag<sup>+</sup> ions. Tan and Chen reported that Tb<sup>3+</sup> luminescence can be increased by 10 folds in the presence of Ag<sup>+</sup>, which allows the detection of Ag<sup>+</sup> down to 60 nM.<sup>[43]</sup> The enhanced energy transfer was believed to be related to the reduction of the fast and competing non-radiative decay of AMP upon Ag<sup>+</sup> bonding. In a reversed system, Shi and co-workers found that Hg<sup>2+</sup> interacts with guanosine and quenches the energy transfer to Tb<sup>3+</sup> in GMP/Tb<sup>3+</sup> nanoparticles.<sup>[44]</sup> Such a Hg-GMP-Tb system can be coupled to cysteine/cystine to probe redox events as thiol-Hg binding restores GMP/Tb<sup>3+</sup> luminescence. The energy donor can also be the entrapped guest molecule in another scenario. Strong Eu<sup>3+</sup>-origin emission can be observed when tetracycline, a popular antibiotic, enters the network of AMP/Eu<sup>3+</sup> assembly.<sup>[45]</sup> Tan *et al.* utilized such a luminescence turn-on behavior to detect tetracycline even in a complicated solution mixture (Figure 13b).<sup>[46]</sup>

Impressively, by loading fluorescent perylene-3,4,9,10-tetracarboxylate to AMP/Gd<sup>3+</sup> nanoparticles, Kimizuka and co-workers found significant dye uptake by the HeLa cells into the lysosomes mediated by the nanoparticles, while the anionic dye alone was not internalized into these cells due to unfavorable electrostatics.<sup>[42b]</sup> When the dye-loaded nanoparticles were injected to mice, accumulation was mostly seen in the liver and low toxicity to liver was found (Figure 13c). Larger species such as Au nanoparticles or proteins can also be immobilized into these supramolecular networks.<sup>[42b]</sup> For the latter, enzymes such as glucose oxidase (GOx) or horse radish peroxidase (HRP) were found to retain their activity and specificity in the trapped in CMP/Eu<sup>3+</sup> nanoparticles.<sup>[42b]</sup>

### 3.2. Porous Crystalline Nucleobase Frameworks

The potential of porous materials that incorporate organic units has been widely explored in the past few decades. Compared to the all inorganic counterparts (*e.g.* zeolites), the rapid growth of all-organic or inorganic-organic hybrid materials leverages the well-developed organic synthesis and understanding in (non-)covalent interactions. To provide scaffolding for the porous network, the organic units should bear suitable functionalities that can engage faithfully in strong (non-)covalent interactions toward multiple directions. This criterion is intrinsically fulfilled with nucleobases due to its variable modes of H-bonding and metal coordination, especially for molecules carrying two or more nucleobases. Additionally, while coordination interactions between metal ions with carboxylate, pyridyl,

or imidazolyl functionality have been widely employed in constructing metal-organic frameworks (MOFs), the less explored yet versatile coordination chemistry of nucleobases can provide opportunity for bio-compatible porous materials.

Adenine (or adeninate, the deprotonated form of A) is by far the most commonly found nucleobase incorporated in MOFs; it coordinates with metal ions through the combination of the N1, N3, N7 or N9 sites in the presence of carboxylate or pyridyl co-ligands.<sup>[12a,47]</sup> It should be noticed that the bidentate N3, N7 coordination from adenine is structurally and electronically similar to carboxylate,<sup>[12c]</sup> a common ligation motif in MOF. Rosi and co-workers, among others, successfully prepared a series of crystalline porous adenine-based MOFs with high surface area<sup>[48]</sup> and unique functionalities.<sup>[12c,49]</sup> For instance, the series of **bio-MOF-11–14**, in which the N3, N7 and N9 sites participate in the Co<sup>2+</sup>-adeninate-carboxylate “paddle-wheel” clusters, have been shown to have high and selective CO<sub>2</sub> uptake (up to 105 cm<sup>3</sup>g<sup>-1</sup> at 298 K, 1 atm) due to the exposed Lewis basic N1 and exocyclic amino groups (Figure 14a).<sup>[47a,50]</sup> High CO<sub>2</sub> capacity (up to 90 cm<sup>3</sup>g<sup>-1</sup>) was also reported for robust **MPM-1** by the Zaworotko group.<sup>[51]</sup> In the latter material, Cu<sup>2+</sup>-adenine (a N7-H tautomer) coordination through the N3 and N9 sites led to discrete dinuclear paddle-wheel complexes [Cu<sub>2</sub>( $\mu$ -adenine)<sub>4</sub>], which further H-bond with the neighbor to construct the framework.

The commonly observed anionic nature of adenine-containing MOF can be used for molecular recognition and drug storage/release. The Rosi group used **bio-MOF-1**, a negatively charged scaffold based on Zn<sub>6</sub>(adeninate)<sub>4</sub>(BPDC)<sub>6</sub> (BPDC = biphenyldicarboxylate, counter ion = Me<sub>2</sub>H<sub>2</sub>N<sup>+</sup>), to host luminescent lanthanide, such as Tb<sup>3+</sup>, Sm<sup>3+</sup>, Eu<sup>3+</sup>, or Yb<sup>3+</sup>, after cation exchange.<sup>[52]</sup> The lanthanide emission is sensitized by excited adenine, akin to the Ln<sup>3+</sup>/AMP adaptive nanoparticles discussed above (Section 3.1), and the variation in luminescent intensity can be used to monitor O<sub>2</sub> concentration. The same MOF is also able to trap cationic procainamide HCl, an antiarrhythmia drug, in its interior. Slow and steady drug release was observed in the PBS buffer; the application of such a system can potentially avoid the frequent drug administration (Figure 14b).<sup>[53]</sup> When some of the binding sites of adenine are not involved in metal coordination, they may be exploited for specific guest recognition in addition to CO<sub>2</sub> adsorptions. Li and co-workers demonstrated such a possibility in **ZnBTCA**, where BTC = benzene-1,3,5-tricarboxylate and A = adenine.<sup>[54]</sup> Similar to the **bio-MOF-11** series,<sup>[50]</sup> adenine's N1 and N3 sites are exposed and available for T binding through the Watson–Crick interaction. Specific uptake of dye molecules with appropriate size and complementary charges in **ZnBTCA** was found; the available H-bonding sites in adenine further causes hysteretic dye uptake/release attributed to mild chemisorption (Figure 14c).<sup>[54]</sup>

The possibility of forming highly ordered porous network without metal coordination was hinted early by the structural elucidation of an ethylene-spaced G:C dinucleoside in solution,<sup>[55]</sup> a G/C base hybrid (pyrido[4,3-*d*]pyrimidine ring skeleton) in the crystal,<sup>[56]</sup> and of a modified G and C nucleobases pairs on the Au(111) surface.<sup>[57]</sup> Following these

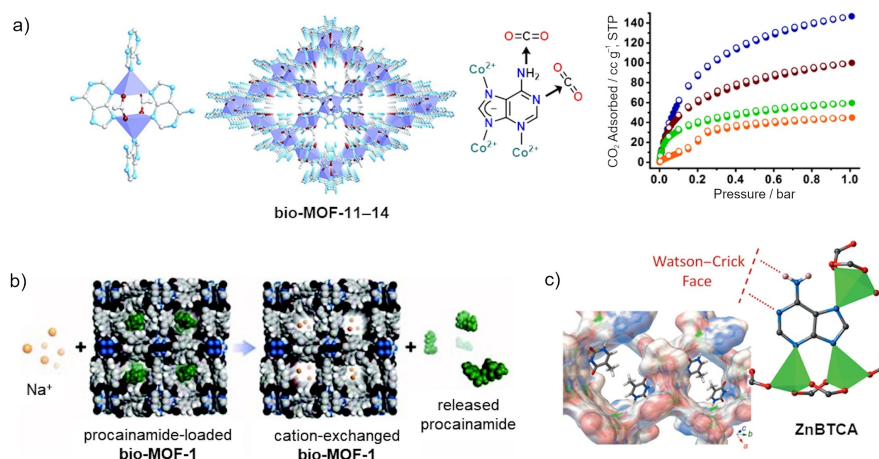


**Figure 14.** a) bio-MOF-11-14 consisting of  $\text{Co}^{2+}$ -adeninate-carboxylates “paddle-wheel” clusters that display high and selective  $\text{CO}_2$  uptake. Reproduced from Ref. [47a] with permission from The Royal Society of Chemistry. b) Cation-triggered procainamide release from a  $\text{Zn}^{2+}$ -adeninate anionic bio-MOF-1. Adapted from Ref. [53] with permission. Copyright (2009) American Chemical Society. c) Exposed H-bonding N1 and N3 sites of adeninate into the pore space in ZnBTCa MOF for guest binding. Adapted from Ref. [54] with permission. Copyright (2015) Wiley-VCH.

studies, recent STM imaging<sup>[58]</sup> of structurally rigid G:C or A:U dinucleobase molecules<sup>[59]</sup> and an equimolar mixture of porphyrins with tetra-A/T groups<sup>[60]</sup> revealed the formation of continuous 2D pores on the highly ordered pyrolytic graphite (HOPG) surface. These structures feature classic Watson–Crick base pairing, and the incorporation of phenylene-ethynylene and porphyrin moieties, common elements in organic electronics, suggests functional materials can be derived using this strategy.

The initial attempts to create porous frameworks using (semi)rigid molecules with multiple nucleobase analogous to Champness' and González-Rodríguez's “crystal tectons”<sup>[58,60]</sup> were proven, however, quite challenging. Weber and co-workers prepared a series of linear or tetrahedral molecules featuring 2 or 4 nucleobases.<sup>[61]</sup> Poor surface areas measured by  $\text{N}_2$  sorption suggested low porosity in these powdery samples, which may be due, in part, to the use of large solubilizing substituents that interfere with expected H-bonding. Nevertheless, these materials showed significant sorption of organic vapors, suggesting available voids in the solids. Such a problem was mitigated slightly when tetrakis(4-thymine)methylphenyl methane or ethylene-9,9'-diadenine was crystallized from 1,1,1,3,3,3-hexafluoro-2-propanol (HFIP) or 2-propanol, respectively.<sup>[62]</sup> The Görbitz group found that very large (up to 67%) unit cell volume was taken by solvents in these crystals; however, the lack of framework structure leads to crystal instability due to loss of solvents.

Recently, Wu and Wasielewski reported guanine-based crystalline organic frameworks.<sup>[63]</sup> Based on the powder X-ray diffraction patterns, the materials are believed to be constructed through H-bonded, metal-free G-quartets.<sup>[64]</sup> The rod-like bis(guaninyl)arene derivatives permits G-quartet formation on both ends of the molecules, resulting in an extended layer of 2D grids that further stack into 3D architecture (Figure 15). The difficulty in handling and crystalizing highly insoluble dinucleobases was circumvented by the use of interim *t*-

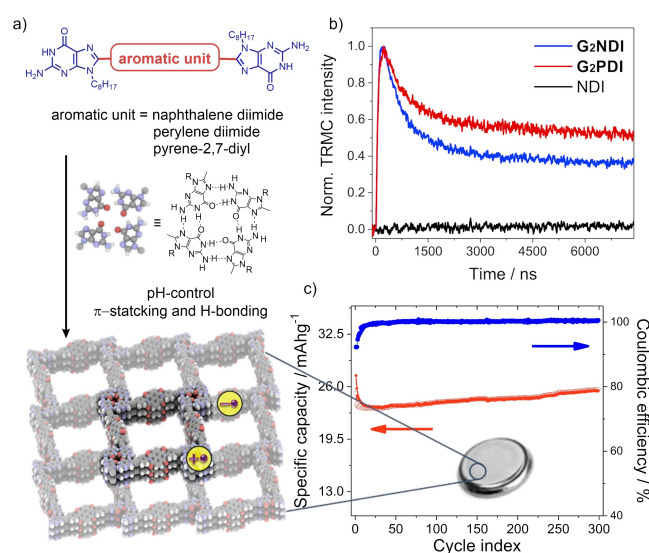


**Figure 15.** a) Crystalline G-quadruplex organic frameworks prepared from linear G-arene-G molecules featuring segregated  $\pi$ -stacks of guanines and arenes for charge-carrier generation, transport, or storage. b) Photogenerated charge-carriers of microsecond lifetime in donor–acceptor G-quadruplex organic frameworks indicated by time-resolved microwave conductivity (TRMC) measurements. c) G<sub>2</sub>PDI organic frameworks as the cathode materials in Li-ion batteries showing high and stable coulombic efficiency over hundreds of recharging cycles.

butyloxycarbonyl (Boc) protecting groups on guanine. The dinucleobases are soluble (in the protonated form) in acidic solution used for trace-less Boc removal; crystallization occurs upon slow reduction of the acidity. The isolation of crystalline frameworks from rod-like bifunctional arenes also suggests that the combination of (i) sterically undemanding and self-ordering alkyl substituents and (ii) rigid and  $\pi$ -stacking aromatic central units are critical to avoid the formation of structurally less defined gels<sup>[65]</sup> or amorphous solids<sup>[61]</sup> from linear dinucleotides. Proper tuning of the strength of  $\pi$ -stacking interaction has been shown imperative for G-quadruplex framework



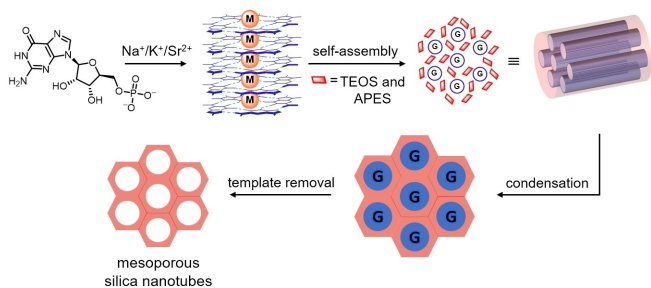


**Figure 16.** Mesoporous silica nanotube formation using G-quadruplex supramolecular structures as the template.

formation.<sup>[63b]</sup> This is made possible in conjunction with slight non-planarity in the aromatic units to restrict interlayer slippage.

The PDI- or NDI-containing G-quadruplex frameworks feature segregated  $\pi$ -stacks of electron-rich G-quadruplex and electron-poor aromatic moieties. Segregation of covalently linked electron donor/acceptor units allows rapid photoinduced charge generation and provides conduit for carrier transport and slow recombination. This was illustrated by the long-lived photo-generated charge carriers, which are mobile within the ordered architecture, based on time-resolved microwave conductivity and EPR measurements.<sup>[63a]</sup> The structural stability of these porous frameworks derived from  $M^+$ -interacting G-quadruplex<sup>[65a,66]</sup> was further found to provide excellent charging/discharging cyclability when the electrochemically active PDI-containing framework was applied as cathode materials in a Li-ion battery.<sup>[63a]</sup>

It is interesting to note that, in the opposite sense to the above porous materials, where nucleobases are part of the backbone of framework architecture, self-assembled G-quadruplexes have been used as supramolecular templates to prepare nano- or mesoporous materials (Figure 16).<sup>[67]</sup> In this approach, the Garcia-Bennett and Xu groups introduced silica source ((3-aminopropyl)triethoxysilane, APES, and tetraethyl orthosilicate, TEOS) to the pre-formed bundles of GMP-quadruplex solutions; electrostatic interaction between the phosphate group in GMP and the amino group in APES induces localization of silica source around the quadruplex for hydrolytic formation of  $\text{SiO}_2$ . Analyses based on powder X-ray diffraction, nitrogen sorption isotherm, and electron microscopy revealed good crystallinity and 1D nano channel in the hydrothermally treated or calcined samples.<sup>[67b,c]</sup>

#### 4. Base-Pairing Interactions in Nucleobase-Functionalized Polymers

Functionalizing polymeric backbones with molecules that are able to provide multiple complementary H-bonding interactions is a well-known field of research in materials science and a large amount of polymers with tuneable properties, due to the reversibility of the H-bond, have been developed.<sup>[68]</sup> Such

macromolecules assembled by noncovalent interactions retain the main features of the native polymers (such as processability or physical/mechanical properties) but additionally endow them with the advantage of smartly changing their properties and/or morphology when exposed to an external stimulus (temperature, mechanical stress, pH or light).

Among many other heteroaromatic compounds available in the literature that exhibit a wide range of association constants,<sup>[69]</sup> the outstanding performance and selectivity of DNA in living systems inspired scientists working in this field to use Watson–Crick base pairing to control polymer structure and properties. However, synthesizing nucleobase-bearing polymers is a challenging process due to the limited solubility and the undesired reactivity of the monomers in certain polymerization methods.<sup>[70]</sup> G and C nucleobases bind strongly, and usually require protecting groups to make their monomer carriers compatible with the polymerization processes. Otherwise, the generated polymers can self-assemble strongly during the polymerization processes, leading to incomplete reactions and insoluble materials. For that reason, it has to be noted that most of the polymers bearing nucleobases developed so far use the A:T(U) pair, as their complementary binding constant is reasonably lower than the G:C pair. The drawback of using this weaker bound base pair is that properties only barely change in comparison with pristine components, particularly in solution. Alternatively, other nucleobase analogues have been installed that replace the natural heterocycles.<sup>[71]</sup> Over the last years, polymer science has explored novel methodologies where milder and more controllable polymerizations processes are utilized,<sup>[72]</sup> which brought to the field different strategies to overcome the problems associated with nucleobase monomer polymerization. Some of these methodologies include ring-opening metathesis polymerization (ROMP), reversible addition–fragmentation chain transfer (RAFT), nitroxide-mediated radical polymerization (NMRP), and atom transfer radical polymerization (ATRP).<sup>[73]</sup>

According to the structural characteristics of the polymers and how the nucleobases are attached to the polymer chain, two main groups of Watson–Crick H-bonded polymer systems can be distinguished. The first group comprises those polymers where the nucleobases are installed at the end of telechelic polymer chains, being able to generate macromolecules with a multiplied molecular weight *via* H-bonding interactions (Figure 17a). In the second, the nucleobases are pendant groups in the main polymer chain, and are synthesized either *via* homo- or copolymerization processes of nucleobase monomers or *via* post-modification of a polymer with reactive side-chain precursors (Figure 17b). In any case, we will highlight in this review the application of Watson–Crick H-bonding interactions to generate particular changes in a target property in polymeric materials by blending complementary nucleobase polymers or low-molecular-weight nucleobases carrying a functional motif.

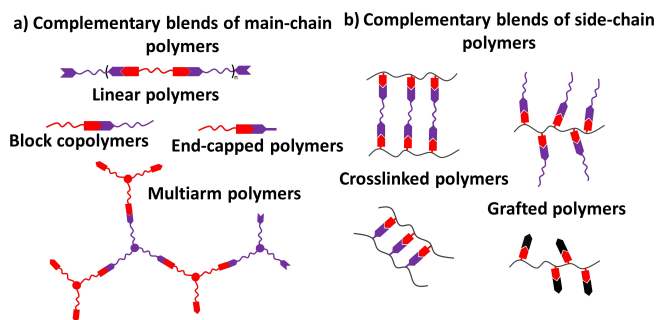


**Figure 17.** Schematic representation of several topologies in nucleobase-functionalized a) main-chain or b) side-chain polymers obtained either by blending the polymers or by combination with cross-linkers/nucleobase carriers.

#### 4.1. Watson–Crick H-bonded Polymer Systems in Solution

Decorating polymer chains with complementary nucleobases can afford a wide range of self-assembled macromolecular systems by the establishment of Watson–Crick interactions. The study of modified nucleobase polymer blends was originally motivated by their potential ability to show DNA-like hybridization, and how this could be exploited in the preparation of supramolecular polymer materials.

One of the very first studies based on the incorporation of complementary nucleobase motifs as pendant groups into polymers blends was developed by the Lutz group.<sup>[74]</sup> They prepared random copolymers of dodecyl methacrylate (DMA) and a styrene carrying A (VBA) or T (VBT) nucleobases. The P(VBT-co-DMA) and P(VBA-co-DMA) copolymers were studied as temperature-responsive materials through UV-vis experiments performed in solvents of decreasing polarity: trifluoroethanol > chloroform > 1,4-dioxane (Figure 18), which had a profound influence on the strength of A:T interactions. Dioxane solutions exhibited the optimal conditions for producing A:T-bound intermolecular assemblies, and a 1:1 mixture of P(VBT-co-DMA) and P(VBA-co-DMA) copolymers formed temperature-dependent supramolecular aggregates, whereas the individual copolymer solutions afforded no response, as shown in Figure 18b–c.

Methacrylic polymers were also used as components in the preparation of nucleobase-bonded materials by Shen and co-workers.<sup>[75]</sup> These authors synthesized A and T monomers (MAT and MAA) (Figure 19a) and the corresponding homopolymers (PMAT and PMAA), and demonstrated a successful self-assembly process between them. Furthermore, a homologue block copolymer P(MAT-*b*-MAA) was able to adopt a “zipper-like” V-shaped configuration through intramolecular H-bonding between the complementary A:T chains in a DMSO/DMF (1:1 v/v) solvent mixture (Figure 19b).<sup>[75]</sup>

Some recent work of Yang and co-workers also highlights the interest in preparing synthetic DNA-like systems with Watson–Crick pairing behavior. They reported polymerization of two types of deoxynucleoside monomers carrying terminal allyl or acryloyl units in the 3'-OH and 5'-OH position, respectively.<sup>[76]</sup> Either non-ordered, regio-uncontrolled or highly ordered, head-to-tail bound oligodeoxynucleosides were ob-

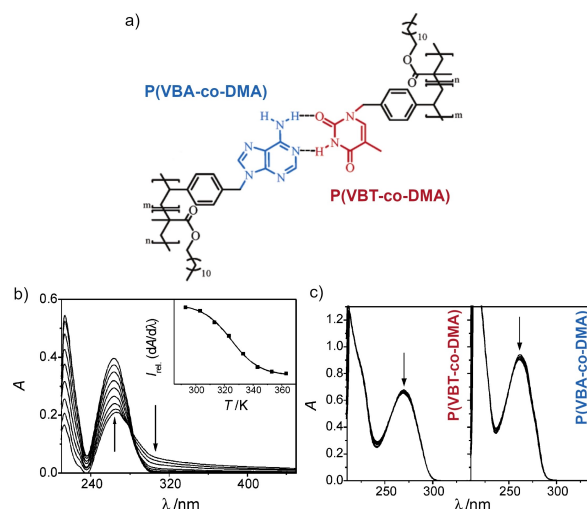


**Figure 18.** a) Structure of the P(VBA-co-DMA) copolymer H-bonded to the complementary P(VBT-co-DMA) copolymer. Temperature-dependent UV-vis experiments of the b) 1:1 A:T copolymers mixture, and c) the individual copolymers in 1,4-dioxane at  $3 \times 10^{-5}$  M. The changes observed upon increasing the temperature are indicated by arrows. The inset on panel b shows the resulting “melting” curve. Adapted from Ref. [74b] with permission. Copyright (2005) American Chemical Society.

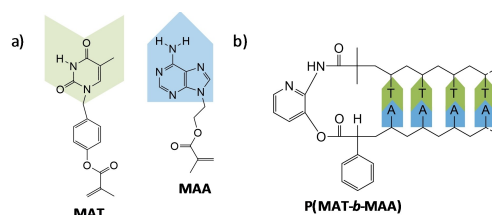


**Figure 19.** a) Chemical structures of the MAT and the MAA monomers. b) Structure of the “zipper-like” P(MAT-*b*-MAA) block copolymer.

tained by subsequent acyclic diene metathesis polymerization (ADMET). These two types of macromolecular architectures significantly influenced the self-assembly morphologies of the oligomers. Spherical nanostructures were obtained with the disordered oligodeoxynucleosides, while well-defined helix fibers were observed when using the ordered oligomers.

Watson–Crick interactions have also been employed to produce linear supramolecular polymer chains from smaller building blocks carrying complementary nucleobases at each terminus. For instance, organic-inorganic hybrid polymers were used by Wu and co-workers to prepare supramolecular polymers based on nucleobase end-capped polyoxometalate (POM) clusters as monomers.<sup>[77]</sup> The monomers consist of symmetrically grafted bifunctional A or T compounds bearing an Anderson-type disk-like  $[\text{MnMo}_6\text{O}_{24}]^{3-}$  cluster (Figure 20). Complementary H-bonding between the nucleobases achieves the formation of a linear polymer, which self-assembles into fibers within several hundred micrometers in length.

The group of Moretto used the same strategy to develop bioinspired  $\alpha$ -aminoisobutyric helical oligopeptide foldamers carrying A- and T- nucleobases in an asymmetric manner at either N- and C- termini.<sup>[78]</sup> The presence of the nucleobases

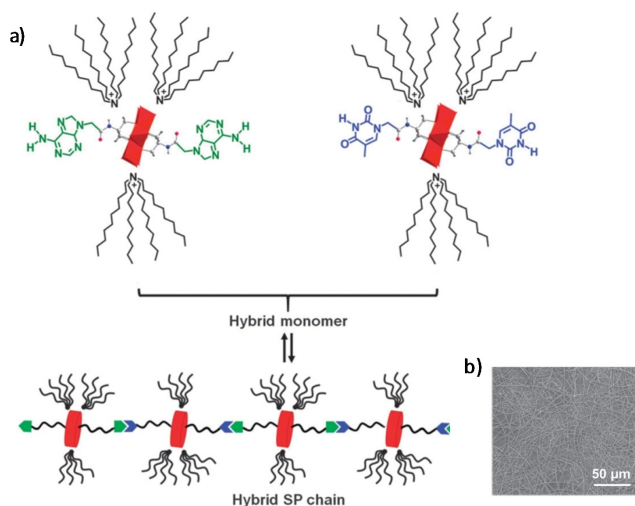


**Figure 20.** a) Schematic illustration of the A- and T-terminated POM monomers and the hybrid supramolecular polymer chain formed through complementary H-bonding between A and T units. b) A SEM image of the polymeric fibers prepared by electrospinning. Reproduced from Ref. [77] with permission from The Royal Society of Chemistry.

allows its precise self-recognition that, combined with intramolecular H-bonding between amino acids, ends up into well-organized supramolecular nanofibers (Figure 21a–b). In order to confirm the role of the nucleobases in polymer formation, they added a “terminator”: the pristine T nucleobase. Depending of

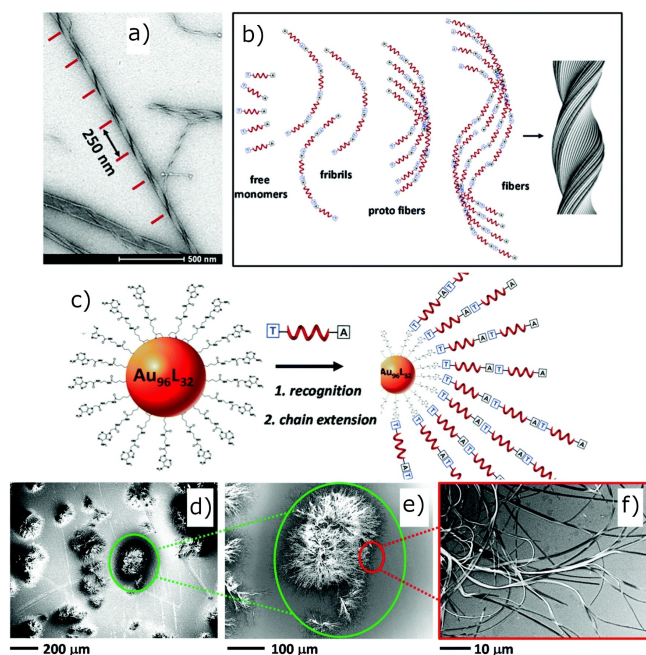


**Figure 21.** a) TEM micrograph highlighting the fiber pitch (scale bar: 500 nm). b) Proposed mechanism of the supramolecular twisted fiber formation from the synthesized α-aminoisobutyric-based foldamers. c) Schematic illustration of the spherical aggregates formed from gold nanoparticles by A:T chain extension. d–f) SEM images of the spherical aggregates obtained with gold nanoparticles with different magnification scales. Reproduced from Ref. [78] with permission from The Royal Society of Chemistry.

the amount of this “T-terminator”, different structural changes in the helical polymer formation were observed, such as length, helicity and density. Moreover, the presence of gold nanoparticles capped with A-motifs on the surface induces the formation of spherical aggregates by recognition and chain extension processes, yielding a functionalized gold nanoparticle core with A:T-based supramolecular polypeptide grafted fibers, as shown in Figure 21c–f. Similarly, Kuo and co-workers prepared supramolecular double-helical structures based on nucleobase interactions stabilized through multiple H-bonds and π–π stacking between pyrene moieties and single-walled carbon nanotubes.<sup>[79]</sup>

Among all self-assembled macromolecular systems produced through the establishment of Watson–Crick interactions, micellar structures obtained in solution (mostly in water) constitute probably the most abundant supramolecular morphology. For instance, the Kuo group prepared a polystyrene-based precursor using the NMRP technique that was then modified with nucleobases by click chemistry giving poly(vinylbenzyl-triazolylmethyl-methylthymine) (PVB-T) and poly(vinylbenzyl-triazolylmethyl-methyladenine) (PVB-A) homopolymers, which stands as an elegant method to prepare complementary polymer chains carrying A and T motifs having exactly the same length. Interestingly, the mixture of PVB-T/PVB-A forms well-controlled spherical aggregates, showing a miscible phase stabilized through multiple complementary H-bonding interactions between nucleobases. The analysis of the resulting reversible supramolecular networks by DSC, rheology, DLS, and TEM confirmed high thermal stability and a high viscosity.<sup>[80]</sup> In a related study, Kuo and co-workers also prepared luminescent polymeric micelles using thymine-modified polycarbazole polymers (PC-T and PTC-T), synthesized through conventional Suzuki coupling polymerization and Cu(I)-catalyzed alkyne/azide cycloaddition reactions.<sup>[81]</sup> These polymers are able to pair with a complementary monofunctional A-terminated poly(ethylene glycol) (PEG-A). The resulting PEG-grafted PC-T/PTC-T polymers self-assembled in water yielding luminescent aggregates of ca. 150 nm diameter, which appeared as polymeric dots with high signal-to-background ratios in fluorescence microscopy.

Recent research has also been focused on studies of micelles obtained from diblock copolymers joining a hydrophilic block (typically poly(ethylene glycol) (PEG)) and a lipophilic block.<sup>[82]</sup> In particular, the incorporation of H-bonding motifs in the hydrophobic segment turned out as a successful strategy in the preparation of polymeric micelles in aqueous media. van Hest and co-workers studied a series of complementary amphiphilic PEG-*b*-PMMA block copolymers, synthesized by ATRP, in which the hydrophobic PMMA block was decorated with A or T fragments (PEG-*b*-A and PEG-*b*-T; Figure 22).<sup>[83]</sup> DLS and UV–Vis measurements proved that the aqueous PEG-*b*-T and PEG-*b*-A mixtures exhibited a significant increase in critical aggregation concentration (CAC), which indicates that A:T interactions enhances aggregation strength. However, a comparison with the isolated PEG-*b*-T and PEG-*b*-A samples showed that the primary self-assembly driving force comes from the hydrophobic nature of the methacrylate backbone.



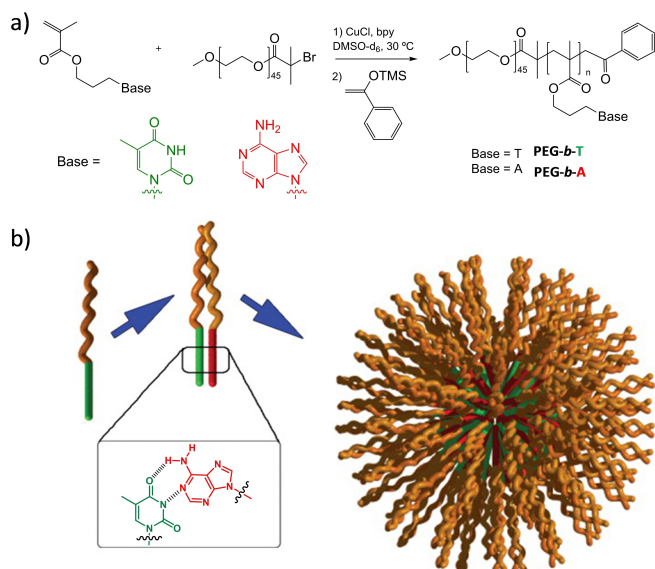


**Figure 22.** a) ATRP procedure for the preparation of the **PEG-b-T** and **PEG-b-A** block copolymers. b) Schematic illustration of the self-assembled complementary **PEG-b-T** and **PEG-b-A** block copolymers. Adapted from Ref. [83] with permission. Copyright (2006) Wiley-VCH.

The O'Reilly group developed polyacrylamide-based complementary block copolymers for the preparation of well-defined supramolecular micelles in DMF/water mixtures, as probed by DLS and TEM.<sup>[84]</sup> Using A- and T-acrylamide monomers (**AAM** and **TAM**) and a poly(4-acryloylmorpholine)-based (**PNA**) macro-CTA, they synthesized **PNA<sub>96</sub>-b-PAAM** and **PNA<sub>96</sub>-b-PTAM** diblock copolymers, respectively, by RAFT polymerization. Different micelle morphologies were achieved through complementary nucleobase interactions by controlling the length of both segments in the copolymers. Moreover, they prepared well-defined micelles from **PNA<sub>96</sub>-b-PAAM<sub>19</sub>** and **PNA<sub>96</sub>-b-PTAM<sub>18</sub>** 1:1 mixtures, that then, upon light-induced [2 + 2] cycloaddition of thymine residues, formed cross-linked spherical particles with an average diameter of  $13 \pm 2$  nm.<sup>[84b]</sup> Later on, the same group reported the preparation of thermoresponsive polymeric nanosized micelles through a supramolecular "grafting-to" approach guided by base-pairing interactions, as shown in Figure 23, by mixing the above described **PNA<sub>96</sub>-b-PTAM** polymer with a series of **PNIPAM-b-PAAM<sub>20</sub>** thermoresponsive diblock copolymers.<sup>[84c]</sup>

When nucleobases are instead installed at the hydrophilic block termini, they accumulate at the micelle surfaces, making them suitable for molecular recognition through Watson-Crick interactions. For instance, Thang and co-workers prepared monofunctional amphiphilic block copolymers by RAFT polymerization that are decorated with A- or T- nucleobases at the hydrophilic segment.<sup>[85]</sup> Such polymers self-assembled into micelles in water, with a diameter range of ca. 100–500 nm, depending on the molecular weight of the copolymers. In addition, temperature-dependent <sup>1</sup>H-NMR experiments proved the controlled release of complementary nucleobase derivatives attached to the surface, due to the reversibility of the A:T bonds.

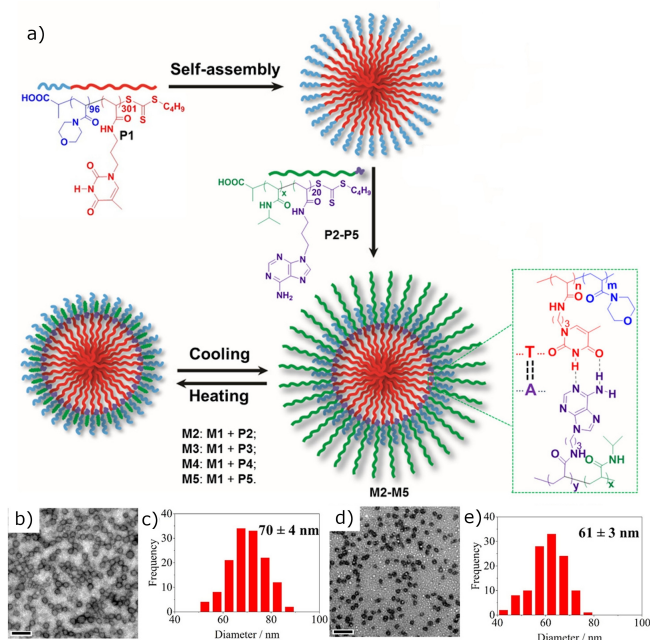


**Figure 23.** a) Schematic procedure of the preparation of supramolecular micelles from mixed-corona polymeric nanostructures through a "Grafting To" approach mediated by nucleobase interactions. TEM images and histograms of number-average diameter distribution of mixed-corona M4 at (b,c) 20 °C and (d,e) 60 °C. Scale bar: 200 nm. Adapted from Ref. [84c] with permission. Copyright (2017) American Chemical Society.

Using a similar strategy, but now combining multifunctional nucleobase hydrophobic polymers and the complementary nucleobase-terminated poly(ethylene oxide) polymer, can also promote micelle formation in water, as Kuo and Zhu (*vide infra*) recently reported. They prepared micelles with the help of the A:T H-bonding interactions from grafted-like supramolecular polymers of poly(styrene-*block*-4-vinylbenzyl-triazolylmethylmethyl-T) (**PS-b-PVBT**) diblock copolymers and an A-terminated poly(ethylene oxide) (**A-PEO**) in DMF. As previously mentioned, the generation of a hydrophobic environment forces H-bonding between nucleobases, and spherical self-assembled objects constituted of a hydrophobic core and a hydrophilic corona are obtained. Controlling the molecular weight of the segments in the copolymers, as well as the microenvironment, allowed the development of multicompartment micelles (Figure 24).<sup>[86]</sup> In this way, they obtained various types of micelles such as raspberry-like spheres, core-shell-corona spheres and cylinders, nanostructured vesicles, onion structures, segmented wormlike cylinders, and woodlouse-like structures (Figure 24b). Such methodology has been proposed as a versatile strategy to prepare potential nanomaterials for biomedical applications, as well as polymeric scaffolds for the synthesis of unprecedented nanosized porous materials.<sup>[86]</sup>

As noncovalent interactions are weak and susceptible to external stimuli, supramolecular polymeric micelles afford novel strategies in the development of highly specific drug delivery systems.<sup>[87]</sup> Specifically, nucleobase-containing polymer micelles have raised as a promising tool in anticancer technologies for their ability to controllably release hydrophobic drugs. Nucleo-

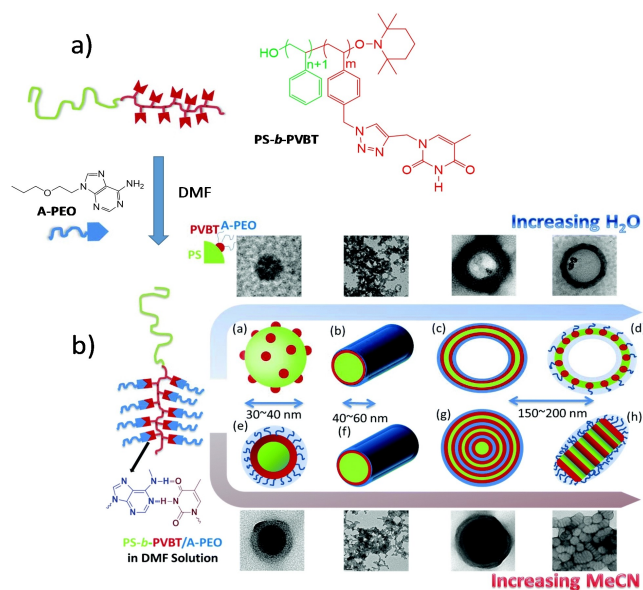


**Figure 24.** a) Schematic illustration of the PS-*b*-PVBT/A-PEO self-assembly process in DMF. b) Multicompartiment micelle structures obtained from the PS-*b*-PVBT/A-PEO blends, depending on the amount of a cosolvent (H<sub>2</sub>O:top or MeCN:bottom). Reproduced from Ref. [86] with permission from The Royal Society of Chemistry.

base association is strongly pH-dependent, which has been used to evaluate the controlled release of anticancer drugs. As it is well known, the pH nearby a tumor is slightly more acidic (pH=6.5) than blood and normal tissues (pH 7.4).<sup>[88]</sup> Taking advantage of this feature, hydrophobic anticancer drugs, such as doxorubicin (DOX),<sup>[89]</sup> were chosen as model compounds to be encapsulated into the hydrophobic core of reversible polymeric micelles. These stable and well-controlled nanostructures, with tuneable sizes comprising from 50 to 200 nm and narrow size distribution, bring numerous advantages, such as improved solubility and availability of hydrophobic drugs in aqueous media, long-term circulation in the bloodstream, and high biocompatibility and targeting capability, among others.

For instance, A:U interactions were used as the noncovalent linker between polymer blocks by Zhu and co-workers, who synthesized the hydrophobic A-terminated poly( $\epsilon$ -caprolactone) (PCL-A) and its complementary hydrophilic U-terminated PEG (PEG-U), with the aim to build supramolecular amphiphilic block copolymers (PCL-A:PEG-U; Figure 25a).<sup>[90]</sup> Due to the amphiphilic nature of the constituents, aside from the multiple A:U H-bonding interactions between them, PCL-A and PEG-U self-assembled in water into micelles (Figure 25c) that exhibited unimodal size distribution and a mean diameter from 142 to 172 nm, depending on the molecular weight of the PCL block (Figure 25b). The supramolecular nanosized conjugates with DOX showed a strong response to moderate acidic media, being able to release the drug inside cells (Figure 25c).

Similarly, the Cheng group recently described the synthesis of a randomly distributed hydrophobic U-PCL copolymer cross-linked *via* U:A interactions with a telechelic PEG decorated with the complementary A base at both termini (BA-PEG; Figure 26).<sup>[91]</sup> This supramolecular network self-assembled in

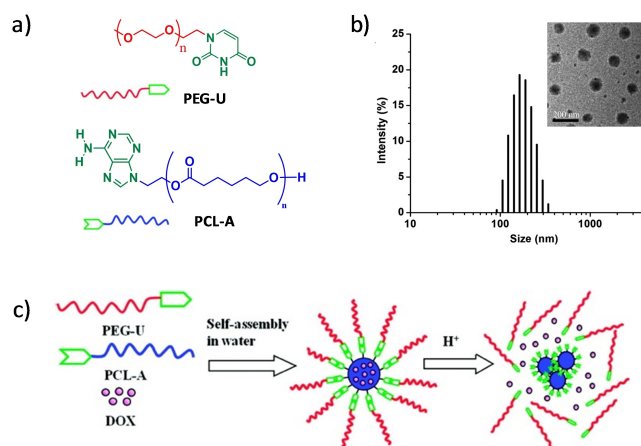


**Figure 25.** a) Chemical structures of the complementary PCL-A and PEG-U block copolymers. b) Size distribution of the self-assembled micelles obtained from the PCL-A/PEG-U mixture determined by DLS, and their corresponding TEM images. c) Scheme of the encapsulation-release process of DOX by the PCL-A/PEG-U entities in water. Adapted from Ref. [90] with permission. Copyright (2011) American Chemical Society.

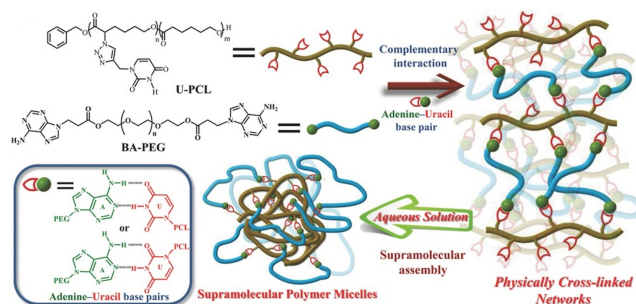


**Figure 26.** Illustration of the cross-linked micelles formed by complementary A:U H-bonding within the U-PCL/BA-PEG copolymer. Reprinted from Ref. [91] with permission. Copyright (2016) Wiley-VCH.

aqueous media into polymeric micelles with a lipophilic core, being able to transport hydrophobic compounds, such as the DOX anticancer drug, and release them at acidic pH.

Huang and co-workers exploited the same strategy for the preparation of pH-responsive drug delivery conjugates based on amphiphilic biodegradable lactide copolymers carrying A and T nucleobases in the hydrophobic portion of the block copolymer,<sup>[92]</sup> mPEG-*b*-P(LA-co-MPA) and mPEG-*b*-P(LA-co-MPT).<sup>[92-93]</sup> The H-bonded A:T hydrophobic core of the carrier is significantly restricting DOX release at physiological pH (7.4). However, the behavior is completely opposite when the pH dropped to 5.0, where the nucleobases are protonated and H-bonding is disrupted. These DOX-loaded polymeric micelles could be internalized by MDA-MB-231 cancer cells and revealed similar anticancer efficacy as free DOX. Other bioinspired degradable polymeric nanocarriers have been reported by the Huang group. They prepared supramolecular micelles that not only disrupt H-bonding in the A:T pair under acidic pH, but also convert a protected dextran hydrophobic segment into hydrophilic dextran through the hydrolysis of the ketal groups.<sup>[94]</sup>

In a related study, Zeng, Wu, and co-workers reported an A-containing P[PEGMA-*b*-(DEMA-co-APMA)]-FA block copolymer that self-assembles at pH 7.4 when mixed with a linear bifunctional U-(CH<sub>2</sub>)<sub>6</sub>-U cross-linker.<sup>[95]</sup> The copolymer forms stable dispersible micelles, which can encapsulate DOX and release this drug at low pH, as a consequence of the disassembly of A:U pairs and protonation of tertiary amines, which led to the concomitant disaggregation of the micelles. Furthermore, the presence of folic acid (FA) at one termini of the hydrophobic segment confers targeting capability to the micelles due to the fact that the folate receptor is overexpressed in several human cancers.<sup>[96]</sup>

Zheng and co-workers described the preparation of H-bonded crosslinked nanoparticles from a polymeric precursor by post-polymerization reactions.<sup>[97]</sup> Specifically, the T-decorated poly(ethylene glycol)-*block*-poly(allyl glycidylether- $\beta$ -mercaptoethanol-thymine) polymer (mPEG-T) and the A-decorated benzyl alcohol-*block*-(poly( $\epsilon$ -caprolactone)-*graft*-poly(2-hydroxyethylacrylate-adenine)) polymer (PCL-A) were mixed in aqueous buffers. This led to supramolecular nanoparticles whose diameter, between *ca.* 10–100 nm, decreased upon lowering the pH from 7.4 to 6.0. A:T pairing was confirmed by <sup>1</sup>H-NMR, and a temperature increase from 25 to 80 °C was enough to break H-bonding interactions. Furthermore, DOX was encapsulated in the hydrophobic core of the nanoparticles, and its release was faster and more effective in acidic media.

Recently, light-responsive nanoparticles based on A:T base pairing were also exploited as controlled drug delivery systems by Song and co-workers.<sup>[98]</sup> "Bionic nanocapsules" of T-modified photoisomerizable polyazobenzene (PETAzO) were obtained by cross-linking with A-modified ZnS (ZnS-A) nanoparticles (NPs) *via* nucleobase pairing. These NPs convert X-rays into UV radiation, which provokes the controlled diffusion of the active drug across the bilayer membranes due to the isomerization of the azobenzene groups. These nanosized entities (*ca.* 100 nm) showed high potential as anticancer drug carriers due to their remotely controlled drug release, prolonged retention, enhanced targeted accumulation, and effective antitumor effects.

Finally, star polymers have also been employed in the generation of micellar systems. A first-generation amphiphilic block copolymer based on multiple Watson–Crick interactions, was developed by Zhu group in collaboration with Su, Guo, and co-workers.<sup>[99]</sup> An A-terminated H<sub>40</sub>-star-poly( $\epsilon$ -caprolactone)-adenine polymer (H<sub>40</sub>PCL-A) and complementary U-monofunctional poly(ethylene glycol) (PEG-U) formed a supramolecular amphiphilic hyperbranched copolymer that self-assembled into pH-responsive micelles in aqueous media with a low CMC (Figure 27a). Diameters between 10 and 200 nm were reached by adjusting the ratio of the two polymeric components (Figure 27b–e).<sup>[99a]</sup> These authors also explored the responsiveness to salt or pH changes of self-assembled brush copolymers micelles prepared from poly(2-hydroxyethylmethacrylate)-*graft*-poly( $\epsilon$ -caprolactone)-adenine (PHEMA-*g*-PCL-A) and the previously describe PEG-U (Figure 28).<sup>[99b]</sup> Low pH or high salt concentration prompted the disassembly of the nanoaggregates, acting as dynamic carriers able to provide fast internalization/release of drugs, which can represent a new generation

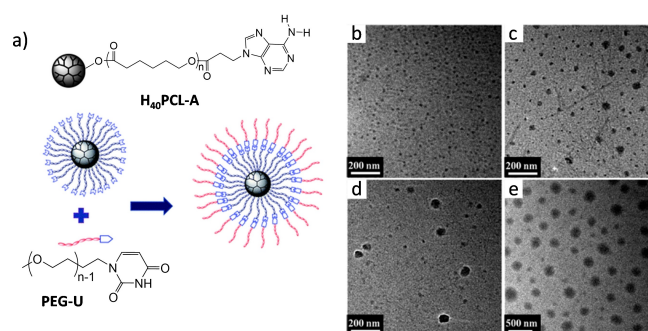


**Figure 27.** a) Scheme of the preparation of the H-bonded H<sub>40</sub>PCL-A/PEG-U multiarm-grafted copolymer micelles. TEM micrographs of the micelles obtained varying the A/U components molar ratio: b) 1:1, c) 1:0.8, d) 1:0.6, and e) 1:0.4. Reproduced from Ref. [99a] with permission from The Royal Society of Chemistry.

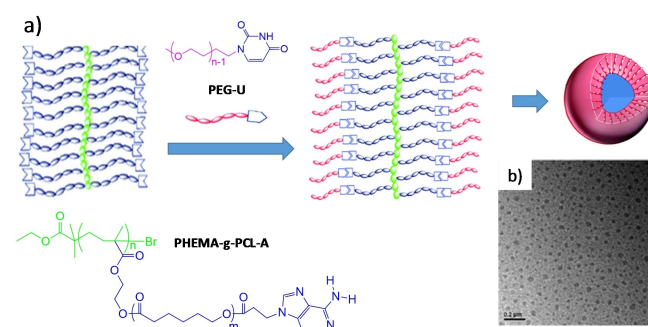


**Figure 28.** a) Schematic illustration of the A:U-based PHEMA-*g*-PCL-A/PEG-U polymer network in water, and its self-assembly into micelles. b) TEM image of the generated micelles (scale bar = 200 nm). Reproduced from Ref. [99b] with permission from The Royal Society of Chemistry.

of stimuli-responsive conjugates for diverse biomedical applications.<sup>[100]</sup>

## 4.2. Watson–Crick Bound Polymer Materials

A main challenge in solid-state supramolecular polymers is to reach optimal mechanical properties while maintaining structural control in a noncovalent reversible architecture. Many efforts have been taken to design H-bonded supramolecular polymers with outstanding features, preserving the reversibility in their constituents. For instance, phase segregation has been exploited as a strategy to successfully improve mechanical properties, such as strength and stiffness, where the segregated hard nano/microp phase stiffens the bulk soft matter.

Nucleobase-pairing has been also used as a tool to develop reinforced phase-segregated polymeric materials. Unsymmetrically substituted telechelic polymers based poly( $\epsilon$ -caprolactone) with A and U residues attached at each edge (A-PCL-U), were synthesized by Chang group through ring-opening polymerization and Michael addition reactions.<sup>[101]</sup> Solid state FT-IR spectroscopy of the self-assembled polymer proved A:U pairing, which led to a dramatic increase of sample viscosity. A lamellar material was formed in which the hard phase



corresponds to the nucleobase pairs at both termini of the polymer chain, which segregates from the PCL central backbone.

Block copolymer synthesis has been exploited as an attractive methodology in which one of the polymer segments bear nucleobase motifs capable of establishing H-bonding associations that leads to self-assembled polymeric materials with unusual properties. Using this strategy, the Kuo group has prepared a self-segregated polymer system by mixing thymine-decorated **PS-*b*-PVBT** block copolymers and the monofunctional 9-hexadecyladenine (**A-C<sub>16</sub>**) (Figure 29a).<sup>[102]</sup> A:T interactions in the blends led to a miscible self-assembled lamellar structure, as confirmed by SAXS and TEM analyses (Figure 29b–

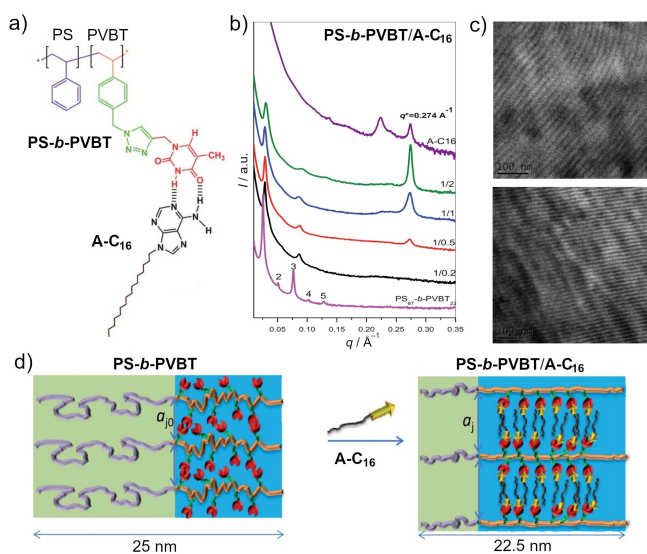


**Figure 29.** a) H-bonded **PS-*b*-PVBT** block copolymer with the **A-C<sub>16</sub>** derivative. b) SAXS patterns of the **PS-*b*-PVBT/A-C<sub>16</sub>** blends at different ratios. c) TEM images of the self-segregated material obtained from the **PS-*b*-PVBT/A-C<sub>16</sub>** 1:0.5 blend, stained with  $I_2/OsO_4$  (top) and  $I_2$  (bottom). d) Representation of the lamellar structures of the **PS-*b*-PVBT** block copolymer and the blend. Reproduced from Ref. [102] with permission from The Royal Society of Chemistry.

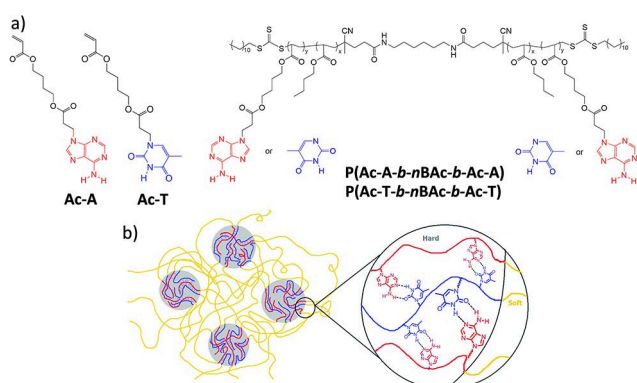


**Figure 30.** a) Structures of the acrylic A- and T-functionalized **Ac-A** and **Ac-T** monomers, and the obtained **P(Ac-A-*b*-nBAC-*b*-Ac-A)** and **P(Ac-T-*b*-nBAC-*b*-Ac-T)** triblock copolymers. b) Graphic illustration of the supramolecular H-bonded complementary triblock copolymers blend. Reproduced from Ref. [104a] - Published by The Royal Society of Chemistry.

c), with polystyrene (PS) lamellar domains (diameter: *ca.* 20–25 nm) in a matrix consisting of the lamellar mesophase (lamellar interdistance: *ca.* 2.3 nm) organized by the **PS-*b*-PVBT/A-C<sub>16</sub>** complex (Figure 29d).

Long and co-workers used the same strategy to attach discrete cationic tetraalkylphosphonium units to triblock copolymers.<sup>[103]</sup> In a more recent study, they have evaluated the role of nucleobase pairing as a driving force in the self-assembly and microphase separation of triblock polyacrylate systems.<sup>[104]</sup> Several glass transition temperatures ( $T_g$ ) in the polymer blends can be used as an indicator of well-separated polymer phases, where hard phases (high  $T_g$ , associated with the external block) and soft phases (low  $T_g$ , associated with the central block) provide mechanical reinforcement and flexibility to the unified material, respectively (Figure 30).<sup>[104a]</sup> The **ABA P(Ac-A-*b*-nBAC-*b*-Ac-A)** and **P(Ac-T-*b*-nBAC-*b*-Ac-T)** triblock copolymers self-segregate into a hard-phase containing acrylic A or T external blocks and a soft-phase containing **BAC** polymer from the central block (Figure 30a). H-bonding between A:T motifs from the external blocks were monitored in the hard-phase by  $^1H$  NMR titration experiments in  $CDCl_3$  at 22 °C, exhibiting an association binding constant of  $K_a = 128 M^{-1}$ . AFM experiments and thermal dynamic-mechanical analysis (DMTA) revealed a well-organized cylindrical microphase-separation of the hard-phase within the PBAC soft-phase, which displays an increase and extension of the  $T_g$  (74 °C) when compared to the  $T_g$  of the isolated components. In addition, the storage modulus of the blend remained virtually stable until *ca.* 82 °C, where a drastic drop was recorded. This represents a difference of about 10–20 °C higher than the thermal transitions of the separated components, and demonstrates that the supramolecular A:T interactions induce a thermally labile, physically cross-linked network that exhibited enhanced mechanical performance with melt processability.<sup>[104a]</sup>

The formation of supramolecular cross-linked polymer networks is a powerful strategy often used to enhance mechanical properties. Numerous research groups focused their investigations on the design of supramolecular polymer networks based on monomers that bear more than two complementary nucleobase H-bonding sites, obtaining highly cross-linked supramolecular networks. For instance, Kuo and co-workers prepared two-component supramolecular homogeneous networks from poly(vinylbenzylthymine-co-butyl methacrylate) and poly(vinylbenzyladenine-co-styrene) random copolymers,<sup>[105]</sup> whereas the original polymers segregate when the multiple H-bonded nucleobases are absent. Apart from SEC, DLS, and viscosity analyses,  $^1H$  NMR and FT-IR experiments suggested that the supramolecular network structures in the blend of both copolymers are indeed stabilized by A:T H-bonding. The Painter–Coleman association model predicted a miscibility window in the blend that arises when the abundance of A:T fragments was higher than 11 mol% in the copolymer composition.

Other than linear polymer chains, Long group used four arm, star-shaped poly(D,L-lactides) (**PDLLAs**) functionalized with complementary A and T nucleobases at the end of the chains.<sup>[106]</sup> H-bonded assemblies of such materials were con-

firmed by  $^1\text{H}$  NMR experiments in  $\text{CDCl}_3$  with a 1:1 optimal stoichiometry, and an association constant of  $K_a = 84 \text{ M}^{-1}$ , within the same order of magnitude of a single A:T pair association. The 1:1 blend showed higher viscosities compared to the pristine polymers, and reversible behavior with temperature with a dramatic drop in the viscosity close to  $100^\circ\text{C}$ . Furthermore, fibers with a substantially higher average diameter can be obtained from the melted or electrospun star-shaped **PDLLA-A** and **PDLLA-T** polymers blended in a 1:1 ratio, in comparison with the pristine materials.<sup>[106b]</sup>

Different approaches for the preparation of supramolecular networks containing polyhedral oligomeric silsesquioxane (**POSS**)<sup>[107]</sup> units have been reported. On one hand, Cheng and co-workers have selected multi-U modified POSS (**POSS-U**) and three-armed PCL oligomers carrying the A motif (**PCL-A**) as complementary blocks (Figure 31a).<sup>[107b]</sup> Moreover, Wu and Kuo prepared multi-functional POSS systems bearing T (**POSS-T**) and A (**POSS-A**) complementary nucleobases (Figure 31b).<sup>[107a]</sup> In any case, the blends of the complementary systems provided strong and reversible multiple H-bonding interactions, either in solution or in the solid state, allowing the preparation of polymer films with promising novel properties, such as thermo-responsiveness or self-healing ability.

A straightforward application of these solid-state H-bonded networks is the use as reversible adhesives. The noncovalent nature of nucleobase-pairing allows the facile disruption of the bonded material upon external stimuli (such as heat, light or pressure) and the debonding on-command. One example of these nucleobase-decorated stimuli responsive adhesives was developed by the Long group.<sup>[108]</sup> Randomly distributed butylacrylate and A-/T-acrylate copolymers were synthesized with different monomer composition, in order to evaluate the role of the self-assembling units in the structural and mechanical properties upon mixing the complementary copolymers. A H-bonded reversible network is formed from the polymer blend

exhibiting temperature-dependent mechanical properties. In particular, a significant improvement in peel and shear strengths was attained in comparison with similar polyacrylates lacking the nucleobase H-bonded motifs (acrylic acid-vinyl-pyridine pairs), which implies potential applications of these materials in coating and adhesive industries.<sup>[109]</sup>

In a related example, the Arimitsu group developed polyacrylate pressure-sensitive adhesives based on A:T binding.<sup>[110]</sup> Specifically, the authors prepared a two-component system constituted by a random copolymer of butylacrylate and T-functionalized acrylate monomers (**P(Act-co-Ac)**) combined with a A-decorated bifunctional low-molecular-weight cross-linker (**A-A**). Dynamic mechanical analysis and stress-strain assays of the blend of both components showed a significant increase of both Young's modulus and  $T_g$  when increasing the amount of crosslinker in the mixture, due to the higher crosslinking density. These facts, along with optimal shear strength, demonstrated adequate adhesive properties of the polymer blend.

In the last years, several research groups have been focused on the preparation of hydrogels for adhesive applications based on supramolecular networks from linear random copolymers using nucleobase pairing for dynamic crosslinking. For instance, Gao and co-workers developed an adhesive material based on A- and T-functionalized polyacrylamide copolymers.<sup>[111]</sup> Comparing with the pristine polyacrylamide hydrogels, these nucleobase H-bonded hydrogels showed improved mechanical properties (twice the value of the maximum strain, and three times the elastic modulus) and better adhesion to different solid materials, including metals, plastics, wood, ceramics, glasses, and biological tissues. Yu and co-workers published the preparation of supramolecular networks of polyphosphoesters cross-linked by A, T and U nucleobases (Figure 32).<sup>[112]</sup> This multiple H-bonded hydrogels exhibited excellent controllable adhesive properties and improved mechanical properties, tackified by nucleobase pairing as demonstrated through rheological measurements. Time sweep profiles showed that both shear elastic and loss moduli increased when the amount of the complementary nucleobases in the polymeric network increased, in comparison with the A-modified polyphosphoesters moduli. Frequency sweep profiles manifested solid-like behavior over the entire frequency range ( $G' > G''$ ), while the moduli dependence on angular frequency dramatically decreased over critical regimes, which suggested the collapse of the supramolecular network due to a transition from gel to a quasi-liquid state. In addition, these hydrogels could be controllably degraded under different pH conditions, while total degradation was achieved in alkaline media due to hydrolysis of phosphoester chains. Cytotoxicity studies indicated that these nucleobase-tackified polyphosphoester-based hydrogels were highly biocompatible, being then an attractive material to be used in biomedical fields that require good mechanical and adhesive properties (such as wound dressing or tissue sealant).

Bioinspired supramolecular hydrogels cross-linked by complementary nucleobases have also found medicinal applications. Telechelic PEG macromers carrying either T or A (**T-PEG-T** and **A-PEG-A**, respectively) were used by Kuang and co-

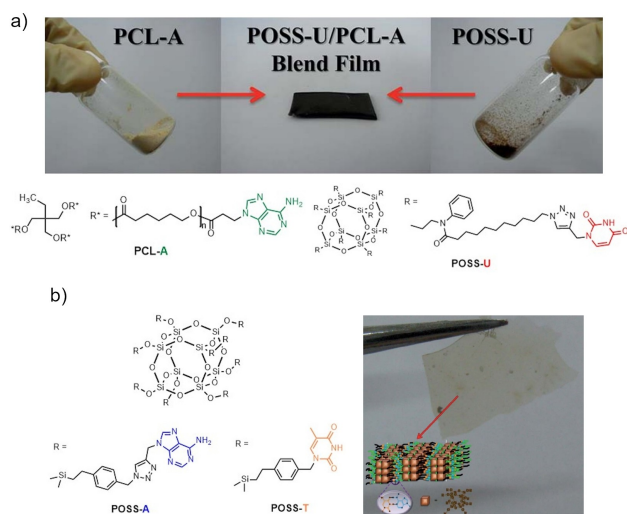


**Figure 31.** a) Polymer film prepared from **POSS-U/PCL-A** blends. b) Polymeric films prepared from 40:60 mixtures of the multifunctional **POSS-T** and **POSS-A**. Reproduced from Ref. [107a–b] with permission from The Royal Society of Chemistry.

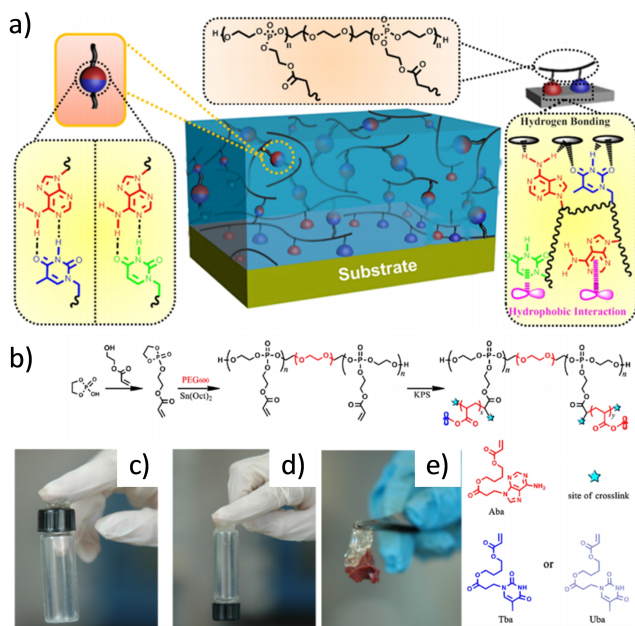


**Figure 32.** (a) Cartoon of the cross-linked hydrogel network, and its adhesion to a substrate driven by nucleobase interactions. (b) Synthesis of polyphosphoester-based hydrogels tackified by nucleobase pairing. c–e) Pictures of the adhered hydrogels to c) plastic, d) glass, and e) fresh live organ of rats. Adapted from Ref. [112] with permission. Copyright (2019) American Chemical Society.

workers.<sup>[113]</sup> They reported the preparation of a biodegradable and injectable supramolecular hydrogel incorporating  $\alpha$ -cyclodextrin ( $\alpha$ -CD; Figure 33). The additive  $\alpha$ -CD threads through the polymers and enhances side interactions between chains, triggering the formation of supramolecular polymer networks, as schematically shown in Figure 33c. This system was success-

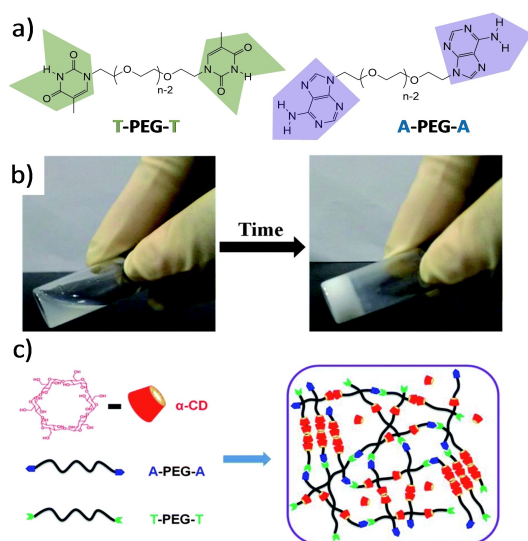


**Figure 33.** a) Chemical structures of the A- and T-functionalized telechelic PEG polymers. b) Pictures of the A-PEG10K-A/T-PEG10K-T/ $\alpha$ -CD aqueous solution (PEG/ $\alpha$ -CD 10:10 weight%) and the hydrogel obtained with time. c) Representation of the gelation process in the mixture of components. Reproduced from Ref. [113] with permission from The Royal Society of Chemistry.

fully tested as a biocompatible and anticancer drug delivery carrier.<sup>[113]</sup>

The Gu group has recently described the preparation of hyaluronic acid-based self-healable hydrogels cross-linked via G:C pairing.<sup>[114]</sup> These G- or C-functionalized hyaluronic acid forms gels in aqueous media with already interesting mechanical properties, that further improved when mixed and complementary base pairing is triggered. These hydrogels have the ability to self-heal with time, and complete dissociation is achieved outside the 6–8 pH window. Moreover, these supramolecular networks showed good biodegradability and effective drug loading and release capacities under physiological conditions.

## 5. Conclusions and Future Remarks

Self-assembling molecular components for bespoke applications requires versatile and reliable organizing platforms as well as a deep understanding of the spatial arrangement of constituting units. Over the years, the vast yet still growing knowledge of supramolecular interactions of nucleobases has offered one of the best apparatus for the design and control of self-assembled architecture. Building on it, the development of nucleobase-derived functional materials is fast evolving; as illustrated in this review, exciting research thrusts span from photosynthetic models, porous materials, chemical sensing, drug delivery, to self-healable and adhesive polymers. From these studies it is clear that the two pairs of complementary nucleobases are more than just additional H-bonding motifs available to the supramolecular chemist. Each purine-pyrimidine pair offers very different hetero-association strengths and selectivities. Besides, they are non-expensive compounds, commercially available in the form of nucleobases, nucleosides, or nucleotides, and have a very rich synthetic chemistry, being among the most widely studied compounds.

While several applications have been demonstrated, it is our believe that the major challenge in maximizing the real-world potential still lies on structural control and characterization. Undoubtedly, the challenge stems from the dynamic nature of supramolecular interactions. On one hand, dynamic and reversible interactions provide means of error correction and self-repair; on the other hand, the “transient” temporal, positional and orientational information of the nucleobases, critical to the property of the self-assemblies, should be critically evaluated. High-resolution microscopies have been increasingly applied to study self-assembled nucleobases. Such resolution is difficult to reach for self-assembled polymeric nucleobase systems. Part of this issue may be alleviated with secondary interactions ( $\pi$ -stacking or co-ligands) to stabilize the supramolecular systems, especially in the presence of competing solvents. Advanced X-ray diffraction and scattering methods, such as pair distribution function analysis (PDF), should provide better structural details within the self-assemblies, particularly suited for those with heavy elements or high crystallinity. Besides the structural dynamics within nucleobase self-assemblies, we also want to point out the importance to



consider how the molecular components react or interface with other species from the system point of view. The consequence of these interaction may include, for instance, modification of supramolecular porosity by chemical reagents and enhanced interfacial charge transport due to properly oriented nucleobases relative to electrodes. Such a control and (in-situ and in-operando) determination, when it is well done, will offer clear design information for a specific application. On the other hand, turning to bio-related applications, nucleobases are biologically compatible compounds, able to interact with other biologically relevant systems like proteins or DNA. There is no doubt that if synthetic self-assembled nucleobase systems could be coupled to DNA technology and (bio)chemistry tools, a wide range of materials with a structural complexity far beyond those of existing materials and exhibiting intriguing and exotic properties, could be created.

## Acknowledgements

Funding from the European Research Council (ERC-Starting Grant 279548 PROGRAM-NANO and ERC-Proof of Concept Grant Poly-Heal 790027) and MINECO (CTQ2017-84727-P) is gratefully acknowledged. A.D.P. acknowledges a Marie Skłodowska-Curie Grant (843090). Y.-L.W. thanks the support from Cardiff University.

## Conflict of Interest

The authors declare no conflict of interest.

**Keywords:** nucleobases · self-assembly · supramolecular chemistry · functional materials · hydrogen bonding

- [1] a) T. Steiner, *Angew. Chem. Int. Ed.* **2002**, *41*, 48–76; *Angew. Chem.* **2002**, *114*, 50–80; b) L. J. Prins, D. N. Reinhoudt, P. Timmerman, *Angew. Chem. Int. Ed.* **2001**, *40*, 2382–2426; *Angew. Chem.* **2001**, *113*, 2446–2492; c) Z.-T. Li, L.-Z. Wu, *Hydrogen bonded supramolecular structures*, Springer, Berlin, **2015**; d) D. Gonzalez-Rodriguez, A. P. H. J. Schenning, *Chem. Mater.* **2011**, *23*, 310–325.
- [2] W. Y. Sun, M. Yoshizawa, T. Kusukawa, M. Fujita, *Curr. Opin. Chem. Biol.* **2002**, *6*, 757–764.
- [3] H. Adams, C. A. Hunter, K. R. Lawson, J. Perkins, S. E. Spey, C. J. Urch, J. M. Sanderson, *Chem. Eur. J.* **2001**, *7*, 4863–4877.
- [4] a) G. R. Desiraju, T. Steiner, *The weak hydrogen bond in structural chemistry and biology*, Oxford University Press, Oxford ; New York, **1999**; b) G. A. Jeffrey, *An introduction to hydrogen bonding*, Oxford University Press, New York, **1997**; c) G. A. Jeffrey, W. Saenger, *Hydrogen bonding in biological structures*, Springer-Verlag, Berlin; New York, **1991**; d) P. Schuster, G. Zundel, C. Sandorfy, *The Hydrogen bond : recent developments in theory and experiments*, North-Holland Pub. Co., Amsterdam ; New York, **1976**.
- [5] E. Arunan, G. R. Desiraju, R. A. Klein, J. Sadlej, S. Scheiner, I. Alkorta, D. C. Clary, R. H. Crabtree, J. J. Dannenberg, P. Hobza, H. G. Kjaergaard, A. C. Legon, B. Mennucci, D. J. Nesbitt, *Pure Appl. Chem.* **2011**, *83*, 1619–1636.
- [6] a) C. A. Hunter, *Angew. Chem. Int. Ed.* **2004**, *43*, 5310–5324; *Angew. Chem.* **2004**, *116*, 5424–5439; b) P. Gilli, L. Pretto, V. Bertolasi, G. Gilli, *Acc. Chem. Res.* **2009**, *42*, 33–44.
- [7] a) S. Sivakova, S. J. Rowan, *Chem. Soc. Rev.* **2005**, *34*, 9–21; b) J. L. Sessler, J. Jayawickramarajah, *Chem. Commun.* **2005**, 1939–1949; c) J. L. Sessler, C. M. Lawrence, J. Jayawickramarajah, *Chem. Soc. Rev.* **2007**, *36*, 314–325; d) M. Fathalla, C. M. Lawrence, N. Zhang, J. L. Sessler, J. Jayawickramarajah, *Chem. Soc. Rev.* **2009**, *38*, 1608–1620; e) C. Montoro-García, M. J. Mayoral, D. González-Rodríguez, *Comprehensive Supramolecular Chemistry II (Ed.: J. Atwood)*, Vol. 4, Elsevier, **2017**; f) P. Zhou, R. Shi, J.-f. Yao, C.-f. Sheng, H. Li, *Coord. Chem. Rev.* **2015**, *292*, 107–143; g) G. M. Peters, J. T. Davis, *Chem. Soc. Rev.* **2016**, *45*, 3188–3206; h) M. Surin, *Polym. Chem.* **2016**, *7*, 4137–4150.
- [8] a) W. L. Jorgensen, J. Pranata, *J. Am. Chem. Soc.* **1990**, *112*, 2008–2010; b) S. C. Van Der Lubbe, F. Zaccaria, X. Sun, C. I. Fonseca Guerra, *J. Am. Chem. Soc.* **2019**, *141*, 4878–4885.
- [9] a) J. T. Davis, *Angew. Chem. Int. Ed.* **2004**, *43*, 668–698; *Angew. Chem.* **2004**, *116*, 684–716; b) J. T. Davis, G. P. Spada, *Chem. Soc. Rev.* **2007**, *36*, 296–313; c) L. Stefan, D. Monchard, *Nat. Rev. Chem.* **2019**, *3*, 650–668.
- [10] a) D. González-Rodríguez, J. L. J. van Dongen, M. Lutz, A. L. Spek, A. P. H. J. Schenning, E. W. Meijer, *Nat. Chem.* **2009**, *1*, 151–155; b) E. Fadaei, M. Martín-Arroyo, M. Tafazzoli, D. González-Rodríguez, *Org. Lett.* **2017**, *19*, 460–463.
- [11] a) M. García-Iglesias, T. Torres, D. González-Rodríguez, *Chem. Commun.* **2016**, *52*, 9446–9449; b) D. González-Rodríguez, P. G. Janssen, R. Martín-Rapún, I. D. Cat, S. D. Feyter, A. P. Schenning, E. Meijer, *J. Am. Chem. Soc.* **2009**, *132*, 4710–4719; c) N. Sreenivasachary, J.-M. Lehn, *Proc. Acad. Sci.* **2005**, *102*, 5938–5943.
- [12] a) S. Verma, A. K. Mishra, A. Kumar, *Acc. Chem. Res.* **2010**, *43*, 79–91; b) B. Lippert, P. J. Sanz Miguel, *Acc. Chem. Res.* **2016**, *49*, 1537–1545; c) G. Beobide, O. Castillo, J. Cepeda, A. Luque, S. Pérez-Yáñez, P. Román, J. Thomas-Gipson, *Coord. Chem. Rev.* **2013**, *257*, 2716–2736; d) P. Amo-Ochoa, F. Zamora, *Coord. Chem. Rev.* **2014**, *276*, 34–58.
- [13] a) E. F. Gomez, A. J. Steckl, *Green Mater. Electron.* **2017**, 191–233; b) E. F. Gomez, V. Venkatraman, J. G. Grote, A. J. Steckl, *Adv. Mater.* **2015**, *27*, 7552–7562.
- [14] a) C. Faber, C. Attacalite, V. Olevano, E. Runge, X. Blase, *Phys. Rev. B* **2011**, *83*; b) J. Lee, J. H. Park, Y. T. Lee, P. J. Jeon, H. S. Lee, S. H. Nam, Y. Yi, Y. Lee, S. Im, *ACS Appl. Mater. Interfaces* **2014**, *6*, 4965–4973; c) C. A. M. Seidel, A. Schulz, M. H. M. Sauer, *J. Phys. Chem.* **1996**, *100*, 5541–5553.
- [15] a) J. L. Sessler, B. Wang, A. Harriman, *J. Am. Chem. Soc.* **1995**, *117*, 704–714; b) N. Armaroli, F. Barigelletti, G. Calogero, L. Flamigni, C. M. White, M. D. Ward, *Chem. Commun.* **1997**, 2181–2182.
- [16] a) T. Forster, *Discuss. Faraday Soc.* **1959**, 7–17; b) D. L. Dexter, *J. Chem. Phys.* **1953**, *21*, 836–850.
- [17] a) P. J. F. Derege, S. A. Williams, M. J. Therien, *Science* **1995**, *269*, 1409–1413; b) C. Turro, C. K. Chang, G. E. Leroi, R. I. Cukier, D. G. Nocera, *J. Am. Chem. Soc.* **1992**, *114*, 4013–4015.
- [18] a) A. Harriman, Y. Kubo, J. L. Sessler, *J. Am. Chem. Soc.* **1992**, *114*, 388–390; b) J. L. Sessler, B. Wang, A. Harriman, *J. Am. Chem. Soc.* **1993**, *115*, 10418–10419.
- [19] J. L. Sessler, J. Jayawickramarajah, A. Gouloumis, T. Torres, D. M. Guldi, S. Maldonado, K. J. Stevenson, *Chem. Commun.* **2005**, 1892–1894.
- [20] J. L. Sessler, J. Jayawickramarajah, A. Gouloumis, G. D. Pantos, T. Torres, D. M. Guldi, *Tetrahedron* **2006**, *62*, 2123–2131.
- [21] J. L. Sessler, M. Sathiosatham, C. T. Brown, T. A. Rhodes, G. Wiederrecht, *J. Am. Chem. Soc.* **2001**, *123*, 3655–3660.
- [22] Z. W. Lin, C. M. Lawrence, D. Q. Xiao, V. V. Kireev, S. S. Skourtis, J. L. Sessler, D. N. Beratan, I. V. Rubtsov, *J. Am. Chem. Soc.* **2009**, *131*, 18060–18062.
- [23] X. Y. Li, D. K. P. Ng, *Tetrahedron Lett.* **2001**, *42*, 305–309.
- [24] Z. Wang, Y. Yu, D. Zhang, D. Zhu, *Chin. Sci. Bull.* **2006**, *51*, 1947–1954.
- [25] F. D'Souza, S. Gadde, D. M. Islam, S. C. Pang, A. L. Schumacher, M. E. Zandler, R. Horie, Y. Araki, O. Ito, *Chem. Commun.* **2007**, 480–482.
- [26] D. M. Guldi, *Chem. Commun.* **2000**, 321–327.
- [27] a) Y. L. Wu, K. E. Brown, M. R. Wasielewski, *J. Am. Chem. Soc.* **2013**, *135*, 13322–13325; b) Y.-L. Wu, K. E. Brown, D. M. Gardner, S. M. Dyar, M. R. Wasielewski, *J. Am. Chem. Soc.* **2015**, *137*, 3981–3990.
- [28] E. Palecek, M. Bartosik, *Chem. Rev.* **2012**, *112*, 3427–3481.
- [29] a) E. Cautet, *J. Biomol. Struct. Dyn.* **2011**, *29*, 557–561; b) J. Choi, J. Park, A. Tanaka, M. J. Park, Y. J. Jang, M. Fujitsuka, S. K. Kim, T. Majima, *Angew. Chem. Int. Ed.* **2013**, *52*, 1134–1138; *Angew. Chem.* **2013**, *125*, 1172–1176; c) S. Delaney, J. K. Barton, *Biochemistry* **2003**, *42*, 14159–14165.
- [30] A. M. Philip, F. Kuriakose, M. Hariharan, *J. Phys. Chem. C* **2017**, *121*, 23259–23267.
- [31] a) D. Porath, G. Cuniberti, R. Di Felice, *Long-Range Charge Transfer in DNA II* **2004**, *237*, 183–227; b) A. R. Arnold, M. A. Grodick, J. K. Barton, *Cell Chem. Biol.* **2016**, *23*, 183–197.

- [32] a) R. Rinaldi, G. Maruccio, A. Biasco, V. Arima, R. Cingolani, T. Giorgi, S. Masiero, G. P. Spada, G. Gottarelli, *Nanotechnology* **2002**, *13*, 398–403; b) G. Maruccio, P. Visconti, V. Arima, S. D'Amico, A. Biasco, E. D'Amone, R. Cingolani, R. Rinaldi, S. Masiero, T. Giorgi, G. Gottarelli, *Nano Lett.* **2003**, *3*, 479–483.
- [33] a) Y. Youn, K. Jung, Y. Lee, S. Park, H. Lee, Y. Yi, *J. Phys. Chem. C* **2017**, *121*, 12750–12756; b) Y. Lee, H. Lee, S. Park, Y. Yi, *Appl. Phys. Lett.* **2012**, *101*, 233305.
- [34] T. Murata, G. Saito, K. Nishimura, Y. Enomoto, G. Honda, Y. Shimizu, S. Matsui, M. Sakata, O. O. Drozdova, K. Yakushi, *Bull. Chem. Soc. Jpn.* **2008**, *81*, 331–344.
- [35] a) Y. Morita, S. Maki, M. Ohmoto, H. Kitagawa, T. Okubo, T. Mitani, K. Nakasuji, *Org. Lett.* **2002**, *4*, 2185–2188; b) T. Murata, E. Miyazaki, S. Maki, Y. Umemoto, M. Ohmoto, K. Nakasuji, Y. Morita, *Bull. Chem. Soc. Jpn.* **2012**, *85*, 995–1006.
- [36] S. J. Choi, J. Kuwabara, T. Kanbara, *Chem. Asian J.* **2010**, *5*, 2154–2157.
- [37] a) S. Alesi, G. Brancolini, I. Viola, M. L. Capobianco, A. Venturini, N. Camaioni, G. Gigli, M. Melucci, G. Barbarella, *Chem. Eur. J.* **2009**, *15*, 1876–1885; b) S. Alesi, G. Brancolini, M. Melucci, M. L. Capobianco, A. Venturini, N. Camaioni, G. Barbarella, *Chem. Eur. J.* **2008**, *14*, 513–521; c) G. P. Spada, S. Lena, S. Masiero, S. Pieraccini, M. Surin, P. Samori, *Adv. Mater.* **2008**, *20*, 2433–2438.
- [38] M. Pandeewar, S. P. Senanayak, T. Govindaraju, *ACS Appl. Mater. Interfaces* **2016**, *8*, 30362–30371.
- [39] Y. Takezawa, M. Shionoya, J. Müller, in *Comprehensive Supramolecular Chemistry II*, **2017**, pp. 259–293.
- [40] a) A. Lopez, J. Liu, *ChemNanoMat* **2017**, *3*, 670–684; b) L. Xu, P. Zhang, Y. Liu, X. Fang, Z. Zhang, Y. Liu, L. Peng, J. Liu, *ACS Omega* **2018**, *3*, 9043–9051.
- [41] A. Ghosh, B. Parasar, T. Bhattacharyya, J. Dash, *Chem. Commun.* **2016**, *52*, 11159–11162.
- [42] a) R. Nishiyabu, C. Aime, R. Gondo, T. Noguchi, N. Kimizuka, *Angew. Chem. Int. Ed.* **2009**, *48*, 9465–9468; *Angew. Chem.* **2009**, *121*, 9629–9632; b) R. Nishiyabu, N. Hashimoto, T. Cho, K. Watanabe, T. Yasunaga, A. Endo, K. Kaneko, T. Niidome, M. Murata, C. Adachi, Y. Katayama, M. Hashizume, N. Kimizuka, *J. Am. Chem. Soc.* **2009**, *131*, 2151–2158.
- [43] H. Tan, Y. Chen, *Chem. Commun.* **2011**, *47*, 12373–12375.
- [44] M. Zhang, Z. B. Qu, C. M. Han, L. F. Lu, Y. Y. Li, T. Zhou, G. Shi, *Chem. Commun.* **2014**, *50*, 12855–12858.
- [45] H. Tan, B. Liu, Y. Chen, *J. Phys. Chem. C* **2012**, *116*, 2292–2296.
- [46] H. Tan, C. Ma, Y. Song, F. Xu, S. Chen, L. Wang, *Biosens. Bioelectron.* **2013**, *50*, 447–452.
- [47] a) T. Li, D.-L. Chen, J. E. Sullivan, M. T. Kozlowski, J. K. Johnson, N. L. Rosi, *Chem. Sci.* **2013**, *4*; b) G. Beobide, O. Castillo, A. Luque, S. Pérez-Yáñez, *CrystEngComm* **2015**, *17*, 3051–3059.
- [48] J. An, O. K. Farha, J. T. Hupp, E. Pohl, J. I. Yeh, N. L. Rosi, *Nat. Commun.* **2012**, *3*, 604.
- [49] a) J. P. García-Teran, O. Castillo, A. Luque, U. Garcia-Couceiro, P. Roman, L. Lezama, *Inorg. Chem.* **2004**, *43*, 4549–4551; b) J. Pascual-Colino, G. Beobide, O. Castillo, I. da Silva, A. Luque, S. Pérez-Yáñez, *Cryst. Growth Des.* **2018**, *18*, 3465–3476.
- [50] J. An, S. J. Geib, N. L. Rosi, *J. Am. Chem. Soc.* **2010**, *132*, 38–39.
- [51] P. S. Nugent, V. L. Rhodus, T. Pham, K. Forrest, L. Wojtas, B. Space, M. J. Zaworotko, *J. Am. Chem. Soc.* **2013**, *135*, 10950–10953.
- [52] J. An, C. M. Shade, D. A. Chengelis-Czegan, S. Petoud, N. L. Rosi, *J. Am. Chem. Soc.* **2011**, *133*, 1220–1223.
- [53] J. Y. An, S. J. Geib, N. L. Rosi, *J. Am. Chem. Soc.* **2009**, *131*, 8376–8377.
- [54] H. Cai, M. Li, X. R. Lin, W. Chen, G. H. Chen, X. C. Huang, D. Li, *Angew. Chem. Int. Ed.* **2015**, *54*, 10454–10459; *Angew. Chem.* **2015**, *127*, 10600–10605.
- [55] J. L. Sessler, J. Jayawickramarajah, M. Sathiosatham, C. L. Sherman, J. S. Brodbelt, *Org. Lett.* **2003**, *5*, 2627–2630.
- [56] M. Mascal, N. M. Hext, R. Warmuth, J. R. Arnall-Culliford, M. H. Moore, J. P. Turkenburg, *J. Org. Chem.* **1999**, *64*, 8479–8484.
- [57] W. Xu, J. G. Wang, M. F. Jacobsen, M. Mura, M. Yu, R. E. Kelly, Q. Q. Meng, E. Laegsgaard, I. Stensgaard, T. R. Linderoth, J. Kjems, L. N. Kantorovich, K. V. Gothelf, F. Besenbacher, *Angew. Chem. Int. Ed.* **2010**, *49*, 9373–9377; *Angew. Chem.* **2010**, *122*, 9563–9567.
- [58] N. Bilbao, I. Destoop, S. De Feyter, D. González-Rodríguez, *Angew. Chem. Int. Ed.* **2016**, *55*, 659–663; *Angew. Chem.* **2016**, *128*, 669–673.
- [59] a) C. Montoro-García, J. Camacho-García, A. M. López-Pérez, N. Bilbao, S. Romero-Pérez, M. J. Mayoral, D. González-Rodríguez, *Angew. Chem. Int. Ed.* **2015**, *54*, 6780–6784; *Angew. Chem.* **2015**, *127*, 6884–6888; b) S. Romero-Pérez, J. Camacho-García, C. Montoro-García, A. M. López-Pérez, A. Sanz, M. J. Mayoral, D. González-Rodríguez, *Org. Lett.* **2015**, *17*, 2664–2667; c) C. Montoro-García, J. Camacho-García, A. M. López-Pérez, M. J. Mayoral, N. Bilbao, D. González-Rodríguez, *Angew. Chem. Int. Ed.* **2016**, *55*, 223–227; *Angew. Chem.* **2016**, *128*, 231–235; d) C. Montoro-García, M. J. Mayoral, R. Chamorro, D. González-Rodríguez, *Angew. Chem. Int. Ed.* **2017**, *56*, 15649–15653; e) C. Montoro-García, N. Bilbao, I. M. Tsagri, F. Zaccaria, M. J. Mayoral, C. Fonseca Guerra, D. González-Rodríguez, *Chem. Eur. J.* **2018**, *24*, 11983–11991; f) R. Chamorro, L. de Juan-Fernández, B. Nieto-Ortega, M. J. Mayoral, S. Casado, L. Ruiz-González, E. M. Pérez, D. González-Rodríguez, *Chem. Sci.* **2018**, *9*, 4176–4184; g) M. J. Mayoral, D. Serrano-Molina, J. Camacho-García, E. Magdalena-Estirado, M. Blanco-Lomas, E. Fadaei, D. González-Rodríguez, *Chem. Sci.* **2018**, *9*, 7809–7821.
- [60] M. O. Blunt, Y. Hu, C. W. Toft, A. G. Slater, W. Lewis, N. R. Champness, *J. Phys. Chem. C* **2018**, *122*, 26070–26079.
- [61] D. Schindler, F. Eissmann, E. Weber, *Org. Biomol. Chem.* **2009**, *7*, 3549–3560.
- [62] a) L. Qi, L. L. Gundersen, C. H. Görbitz, *CrystEngComm* **2018**, *20*, 1179–1184; b) L. Qi, L. L. Gundersen, E. J. Chamgordani, C. H. Görbitz, *CrystEngComm* **2016**, *18*, 6352–6357.
- [63] a) Y. L. Wu, N. E. Horwitz, K. S. Chen, D. A. Gomez-Gualdrón, N. S. Luu, L. Ma, T. C. Wang, M. C. Hersam, J. T. Hupp, O. K. Farha, R. Q. Snurr, M. R. Wasielewski, *Nat. Chem.* **2017**, *9*, 466–472; b) Y.-L. Wu, N. S. Bobbitt, J. L. Logsdon, N. E. Powers-Riggs, J. N. Nelson, X. L. Liu, T. C. Wang, R. Q. Snurr, J. T. Hupp, O. K. Farha, M. C. Hersam, M. R. Wasielewski, *Angew. Chem. Int. Ed.* **2018**, *57*, 3985–3989; *Angew. Chem.* **2018**, *130*, 4049–4053.
- [64] a) R. Otero, M. Schöck, L. M. Molina, E. Laegsgaard, I. Stensgaard, B. Hammer, F. Besenbacher, *Angew. Chem. Int. Ed.* **2005**, *44*, 2270–2275; *Angew. Chem.* **2005**, *117*, 2310–2315; b) J. L. Sessler, M. Sathiosatham, K. Doerr, V. Lynch, K. A. Abboud, *Angew. Chem. Int. Ed.* **2000**, *39*, 1300–1303; *Angew. Chem.* **2000**, *112*, 1356–1359.
- [65] a) C. Arnal-Herault, A. Pasc, M. Michau, D. Cot, E. Petit, M. Barboiu, *Angew. Chem. Int. Ed.* **2007**, *46*, 8409–8413; *Angew. Chem.* **2007**, *119*, 8561–8565; b) T. Shimizu, R. Iwaura, M. Masuda, T. Hanada, K. Yase, *J. Am. Chem. Soc.* **2001**, *123*, 5947–5955; c) H. H. Kuang, H. Y. He, Z. Y. Zhang, Y. X. Qi, Z. G. Xie, X. B. Jing, Y. B. Huang, *J. Mater. Chem. B* **2014**, *2*, 659–667.
- [66] S. L. Forman, J. C. Fettinger, S. Pieraccini, G. Gottarelli, J. T. Davis, *J. Am. Chem. Soc.* **2000**, *122*, 4060–4067.
- [67] a) C. Arnal-Herault, A. Banu, M. Barboiu, M. Michau, A. van der Lee, *Angew. Chem. Int. Ed.* **2007**, *46*, 4268–4272; *Angew. Chem.* **2007**, *119*, 4346–4350; b) L. Min, T. Li, Q. Tan, X. Tan, W. Pan, L. He, J. Zhang, E. Ou, W. Xu, *Dalton Trans.* **2016**, *45*, 7912–7920; c) C. J. Bueno-Alejo, L. A. Villaescusa, A. E. Garcia-Bennett, *Angew. Chem. Int. Ed.* **2014**, *53*, 12106–12110; *Angew. Chem.* **2014**, *126*, 12302–12306.
- [68] a) L. Brunsveld, B. Folmer, E. W. Meijer, R. Sijbesma, *Chem. Rev.* **2001**, *101*, 4071–4098; b) T. F. De Greef, M. M. Smulders, M. Wolfs, A. P. Schenning, R. P. Sijbesma, E. Meijer, *Chem. Rev.* **2009**, *109*, 5687–5754; c) E. Krieg, M. M. Bastings, P. Besenius, B. Rybtchinski, *Chem. Rev.* **2016**, *116*, 2414–2477.
- [69] a) S. K. Yang, S. C. Zimmerman, *Isr. J. Chem.* **2013**, *53*, 511–520; b) A. J. Wilson, *Soft Matter* **2007**, *3*, 409–425.
- [70] a) R. McHale, R. K. O'Reilly, *Macromolecules* **2012**, *45*, 7665–7675; b) S. T. Hemp, T. E. Long, *Macromol. Biosci.* **2012**, *12*, 29–39; c) P. K. Lo, H. F. Sleiman, *Macromolecules* **2008**, *41*, 5590–5603; d) P. K. Lo, H. F. Sleiman, *J. Am. Chem. Soc.* **2009**, *131*, 4182–4183.
- [71] A. K. Boal, F. Ilhan, J. E. DeRouche, T. Thurn-Albrecht, T. P. Russell, V. M. Rotello, *Nature* **2000**, *404*, 746.
- [72] a) M. A. Tasdelen, M. U. Kahveci, Y. Yagci, *Prog. Polym. Sci.* **2011**, *36*, 455–567; b) M. Beija, M.-T. Charreyre, J. M. Martinho, *Prog. Polym. Sci.* **2011**, *36*, 568–602; c) A. Anastasaki, V. Nikolaou, G. Nurumbetov, P. Wilson, K. Kempe, J. F. Quinn, T. P. Davis, M. R. Whittaker, D. M. Haddleton, *Chem. Rev.* **2015**, *116*, 835–877; d) T. E. Patten, K. Matyjaszewski, *Adv. Mater.* **1998**, *10*, 901–915; e) K. Matyjaszewski, J. Xia, *Chem. Rev.* **2001**, *101*, 2921–2990; f) J.-F. Lutz, M. Ouchi, D. R. Liu, M. Sawamoto, *Science* **2013**, *341*, 1238149.
- [73] a) A. Marsh, A. Khan, D. M. Haddleton, M. J. Hannon, *Macromolecules* **1999**, *32*, 8725–8731; b) H. J. Spijker, F. L. van Delft, J. C. van Hest, *Macromolecules* **2007**, *40*, 12–18; c) M. Kato, M. Kamigaito, M. Sawamoto, T. Higashimura, *Macromolecules* **1995**, *28*, 1721–1723.
- [74] a) J.-F. Lutz, A. F. Thünemann, R. Nehring, *J. Polym. Sci. Part A* **2005**, *43*, 4805–4818; b) J.-F. Lutz, A. F. Thünemann, K. Rurack, *Macromolecules* **2005**, *38*, 8124–8126; c) J.-F. Lutz, S. Pfeifer, M. Chanana, A. F. Thünemann, R. Bienert, *Langmuir* **2006**, *22*, 7411–7415.

- [75] H. Tang, M. Radosz, Y. Shen, *J. Polym. Sci. Part A* **2006**, *44*, 5995–6006.
- [76] L. Wang, M. Wang, L.-X. Guo, Y. Sun, X.-Q. Zhang, B.-P. Lin, H. Yang, *Macromolecules* **2019**, *52*, 649–659.
- [77] Z. He, B. Li, H. Ai, H. Li, L. Wu, *Chem. Commun.* **2013**, *49*, 8039–8041.
- [78] G. Marafon, I. Menegazzo, M. De Zotti, M. Crisma, C. Toniolo, A. Moretto, *Soft Matter* **2017**, *13*, 4231–4240.
- [79] K.-W. Huang, Y.-R. Wu, K.-U. Jeong, S.-W. Kuo, *Macromol. Rapid Commun.* **2013**, *34*, 1530–1536.
- [80] Y.-S. Wu, Y.-C. Wu, S.-W. Kuo, *Polymer* **2014**, *6*, 1827–1845.
- [81] C.-W. Huang, W.-Y. Ji, S.-W. Kuo, *Macromolecules* **2017**, *50*, 7091–7101.
- [82] J. A. Opsteen, J. J. Cornelissen, J. C. Van Hest, *Pure Appl. Chem.* **2004**, *76*, 1309–1319.
- [83] H. J. Spijker, A. J. Dirks, J. C. M. van Hest, *J. Polym. Sci. Part A* **2006**, *44*, 4242–4250.
- [84] a) Z. Hua, A. Pitto-Barry, Y. Kang, N. Kirby, T. R. Wilks, R. K. O'Reilly, *Polym. Chem.* **2016**, *7*, 4254–4262; b) Z. Hua, T. R. Wilks, R. Keogh, G. Herwig, V. G. Stavros, R. K. O'Reilly, *Chem. Mater.* **2018**, *30*, 1408–1416; c) Z. Hua, R. Keogh, Z. Li, T. R. Wilks, G. Chen, R. K. O'Reilly, *Macromolecules* **2017**, *50*, 3662–3670.
- [85] M. Wang, B. Choi, X. Wei, A. Feng, S. H. Thang, *Polym. Chem.* **2018**, *9*, 5086–5094.
- [86] Y.-C. Wu, B. Prasad Bastakoti, M. Pramanik, Y. Yamauchi, S.-W. Kuo, *Polym. Chem.* **2015**, *6*, 5110–5124.
- [87] a) Z. Ge, S. Liu, *Chem. Soc. Rev.* **2013**, *42*, 7289–7325; b) S. Mura, J. Nicolas, P. Couvreur, *Nat. Mater.* **2013**, *12*, 991–1003; c) J. Ding, L. Chen, C. Xiao, L. Chen, X. Zhuang, X. Chen, *Chem. Commun.* **2014**, *50*, 11274–11290.
- [88] D. M. Prescott, H. C. Charles, J. M. Poulson, R. L. Page, D. E. Thrall, Z. Vujaskovic, M. W. Dewhirst, *Clin. Cancer Res.* **2000**, *6*, 2501–2505.
- [89] F. Meng, Y. Zhong, R. Cheng, C. Deng, Z. Zhong, *Nanomedicine* **2014**, *9*, 487–499.
- [90] D. Wang, Y. Su, C. Jin, B. Zhu, Y. Pang, L. Zhu, J. Liu, C. Tu, D. Yan, X. Zhu, *Biomacromolecules* **2011**, *12*, 1370–1379.
- [91] C.-C. Cheng, I.-H. Lin, J.-K. Chen, Z.-S. Liao, J.-J. Huang, D.-J. Lee, Z. Xin, *Macromol. Biosci.* **2016**, *16*, 1415–1421.
- [92] H. Kuang, S. Wu, F. Meng, Z. Xie, X. Jing, Y. Huang, *J. Mater. Chem.* **2012**, *22*, 24832–24840.
- [93] a) H. Kuang, S. Wu, Z. Xie, F. Meng, X. Jing, Y. Huang, *Biomacromolecules* **2012**, *13*, 3004–3012; b) X. Zhang, Z. He, G. Li, Y. Zhang, G. Li, *J. Polym. Res.* **2010**, *17*, 255–263.
- [94] H. Kuang, Y. Wu, Z. Zhang, J. Li, X. Chen, Z. Xie, X. Jing, Y. Huang, *Polym. Chem.* **2015**, *6*, 3625–3633.
- [95] J. Fan, F. Zeng, S. Wu, X. Wang, *Biomacromolecules* **2012**, *13*, 4126–4137.
- [96] H. Xu, H. Ma, P. Yang, X. Zhang, X. Wu, W. Yin, H. Wang, D. Xu, *Colloids Surf. B* **2015**, *136*, 729–734.
- [97] X. Zhao, H. Deng, H. Feng, J. Zhang, A. Dong, L. Deng, *Macromol. Chem. Phys.* **2016**, *217*, 2611–2616.
- [98] Y. Yoon, A. P. Tiwari, M. Choi, T. G. Novak, W. Song, H. Chang, T. Zyung, S. S. Lee, S. Jeon, K.-S. An, *Adv. Funct. Mater.* **2019**, *29*, 1903443.
- [99] a) D. Wang, H. Chen, Y. Su, F. Qiu, L. Zhu, X. Huan, B. Zhu, D. Yan, F. Guo, X. Zhu, *Polym. Chem.* **2013**, *4*, 85–94; b) D. Wang, X. Huan, L. Zhu, J. Liu, F. Qiu, D. Yan, X. Zhu, *RSC Adv.* **2012**, *2*, 11953–11962.
- [100] D. Wang, T. Zhao, X. Zhu, D. Yan, W. Wang, *Chem. Soc. Rev.* **2015**, *44*, 4023–4071.
- [101] I.-H. Lin, C.-C. Cheng, Y.-C. Yen, F.-C. Chang, *Macromolecules* **2010**, *43*, 1245–1252.
- [102] Y.-C. Wu, S.-W. Kuo, *Polym. Chem.* **2012**, *3*, 3100–3111.
- [103] B. D. Mather, M. B. Baker, F. L. Beyer, M. D. Green, M. A. G. Berg, T. E. Long, *Macromolecules* **2007**, *40*, 4396–4398.
- [104] a) K. Zhang, M. Aiba, G. B. Fahs, A. G. Hudson, W. D. Chiang, R. B. Moore, M. Ueda, T. E. Long, *Polym. Chem.* **2015**, *6*, 2434–2444; b) B. D. Mather, M. B. Baker, F. L. Beyer, M. A. G. Berg, M. D. Green, T. E. Long, *Macromolecules* **2007**, *40*, 6834–6845; c) K. Zhang, G. B. Fahs, M. Aiba, R. B. Moore, T. E. Long, *Chem. Commun.* **2014**, *50*, 9145–9148.
- [105] S.-W. Kuo, R.-S. Cheng, *Polymer* **2009**, *50*, 177–188.
- [106] a) A. S. Karikari, B. D. Mather, T. E. Long, *Biomacromolecules* **2007**, *8*, 302–308; b) M. T. Hunley, A. S. Karikari, M. G. McKee, B. D. Mather, J. M. Layman, A. R. Fornof, T. E. Long, *Macromol. Symp.* **2008**, *270*, 1–7.
- [107] a) Y.-C. Wu, S.-W. Kuo, *J. Mater. Chem.* **2012**, *22*, 2982–2991; b) C.-C. Cheng, F.-C. Chang, S. A. Dai, Y.-L. Lin, D.-J. Lee, *RSC Adv.* **2015**, *5*, 90466–90472; c) J.-H. Jeon, T. Kakuta, K. Tanaka, Y. Chujo, *Bioorg. Med. Chem. Lett.* **2015**, *25*, 2050–2055.
- [108] S. Cheng, M. Zhang, N. Dixit, R. B. Moore, T. E. Long, *Macromolecules* **2012**, *45*, 805–812.
- [109] C. Heinzmann, C. Weder, L. M. de Espinosa, *Chem. Soc. Rev.* **2016**, *45*, 342–358.
- [110] a) N. Ishikawa, M. Furutani, K. Arimitsu, *ACS Macro Lett.* **2015**, *4*, 741–744; b) N. Ishikawa, M. Furutani, K. Arimitsu, *J. Polym. Sci. Part A* **2016**, *54*, 1332–1338.
- [111] X. Liu, Q. Zhang, Z. Gao, R. Hou, G. Gao, *ACS Appl. Mater. Interfaces* **2017**, *9*, 17645–17652.
- [112] W. Wang, S. Liu, B. Chen, X. Yan, S. Li, X. Ma, X. Yu, *Biomacromolecules* **2019**, *20*, 3672–3683.
- [113] H. Kuang, H. He, Z. Zhang, Y. Qi, Z. Xie, X. Jing, Y. Huang, *J. Mater. Chem. B* **2014**, *2*, 659–667.
- [114] X. Ye, X. Li, Y. Shen, G. Chang, J. Yang, Z. Gu, *Polymer* **2017**, *108*, 348–360.

Manuscript received: December 17, 2019  
Revised manuscript received: March 5, 2020